Tectonic Topography Changes in Cenozoic East Asia: A Landscape Erosion-Sediment Archive in the South China Sea

Yi Yan[1] [ID], Deng Yao[1,2], Zhi-Xian Tian[1], Chi-Yue Huang[1] [ID], Yildirim Dilek[3] [ID], Peter D. Clift[4] [ID], and Zi-An Li[5]

[1]Key Laboratory of Ocean and Marginal Sea Geology, Guangzhou Institute of Geochemistry, Chinese Academy of Sciences, Guangzhou, China, [2]College of Earth and Planetary Sciences, University of Chinese Academy of Sciences, Beijing, China, [3]Department of Geology & Environmental Earth Science, Miami University, OH, USA, [4]Department of Geology and Geophysics, Louisiana State University, Baton Rouge, LA, USA, [5]School of Marine Sciences, Sun Yat-Sen University, Guangzhou, China

Abstract The mode and tempo of Cenozoic fluvial input into the South China Sea by Asian rivers were strongly controlled by tectonically induced topographic changes and landscape development that resulted in repeated river captures and reversals. New Nd isotope and U-Pb detrital zircon data from clastic sedimentary sequences in the northern South China Sea display secular variations reflecting significant changes in the compositions of fluvial sediment as well as changes in source rocks. The oldest, Eocene-Oligocene (before ∼25 Ma) clastic rocks of the South China Sea contain sediments with ε_{Nd} values of −5 to −7.5 and detrital zircons of Cretaceous, Jurassic, and Permo-Triassic, all derived from southern Cathaysia. The Oligocene-Middle Miocene (∼25–11 Ma) sediments in the South China Sea strata display ε_{Nd} values of −12 to −14 and Archean, Proterozoic, and Paleozoic detrital zircons, suggesting northern Cathaysia and/or the Yangtze Blocks as their provenance. The headward expansion of the Pearl River and reversal of the Middle Yangtze River correlates with the opening of the South China Sea and growth of the eastern Tibetan Plateau at ∼25 Ma. Further uplift of the eastern Tibetan Plateau and the Wuyi-Nanling Mountains in SE China around 11 Ma reshaped the landscape and caused another phase of erosion—pattern adjustment and drainage—divide migration in East Asia, leading to the establishment of the modern fluvial systems of the Pearl, Minjiang, and Lower Yangtze Rivers.

Plain Language Summary The mode and tempo of Cenozoic fluvial input into the South China Sea by Asian rivers were strongly controlled by tectonically induced topographic changes and landscape development that resulted in repeated river captures and reversals. This study reconstructs tectonic topography changes and drainage development over 30 million years using Nd isotope and single grain zircon U-Pb data from the South China Sea. Our study shows that tectonic topography and river systems in East Tibet experienced two major reorganization events, reflecting the protracted and episodic growth of eastern Tibet, East Asia marginal seas, and Asian monsoonal climate. Our findings shed light on how tectonic, climate, and river drainage processes have interacted in this part of the world during the latter part of the Cenozoic. We believe our work is international interest and contributed to unravel the history of tectonic topographic evolution and drainage development through time in eastern Tibet.

1. Introduction

The tectonics associated with spreading of the East Asian marginal sea and uplift of the eastern margin of the Tibetan Plateau exerted important influence on the topography and drainage system in East Asia (Clark et al., 2005; Clift et al., 2006a; Kirby et al., 2002; Lan et al., 2014; Richardson et al., 2010; Zhang et al., 2017; Zheng et al., 2013). The South China Sea was formed by oceanic spreading at ∼30 Ma (Briais et al., 1993) following an extended period of extension dating back to at least Eocene (Ru & Pigott, 1986). Thermochronological data suggest that the eastern margin of the Tibetan Plateau experienced rapid exhumation beginning at 30–25 Ma (Tapponnier et al., 2001; Wang et al., 2012) and continued fast erosion during Late Miocene (Clark et al., 2005; Kirby et al., 2002). Late Mesozoic granites are extensively exposed along the south-eastern margin of the South China Block, suggesting that kilometer-scale erosion has occurred since the Late Mesozoic (Yan et al., 2009).

In SE, Tibet several large rivers including the Yangtze and Red Rivers run close together. It has been proposed that this reflects horizontal compression of the area following India-Asia collision (Brookfield, 1998). However, this is now more argued to be a result of large-scale headwater capture as the Tibetan plateau experienced surface uplift (Clift et al., 2006a). The drainage evolution is important to constrain the surface uplift of the eastern Tibetan Plateau and the topographic reversal in East Asia. However, the timing and nature of river drainage evolution remains debateable (Clift et al., 2006a; Richardson et al., 2010; Yang et al., 2006; Zheng et al., 2013). Although several studies suggest a significant change in river drainage patterns occurred at around 24 Ma, this conclusion is only weakly supported (Clift et al., 2006a; Zheng et al., 2013). Previous investigations largely focused on records in terrestrial strata, which faced limitations from the discontinuous accumulation and ambiguous depositional ages (Clift et al., 2006a; Zheng et al., 2013). In fact, the sedimentary record from the Yangtze River and other major river systems in SE China together with data from the South China Sea demonstrate that the regional river drainage patterns were likely to have reorganized multiple times (Clift et al., 2006a; Hoang et al., 2009; Lan et al., 2014).

The drainage systems of southern China, such as the Pearl and Minjiang Rivers drain much of mainland SE Asia and have resulted in the deposition of km-thick clastic sediments in the northern margin of the South China Sea (Figure 1). However, the evolution of the Pearl and Minjiang Rivers has been generally overlooked. The relationship between the Yangtze River and the Pearl and Minjiang Rivers is ambiguous. How uplift of the eastern Tibetan Plateau and opening of marginal sea affect landscape changes and river system evolution is unclear.
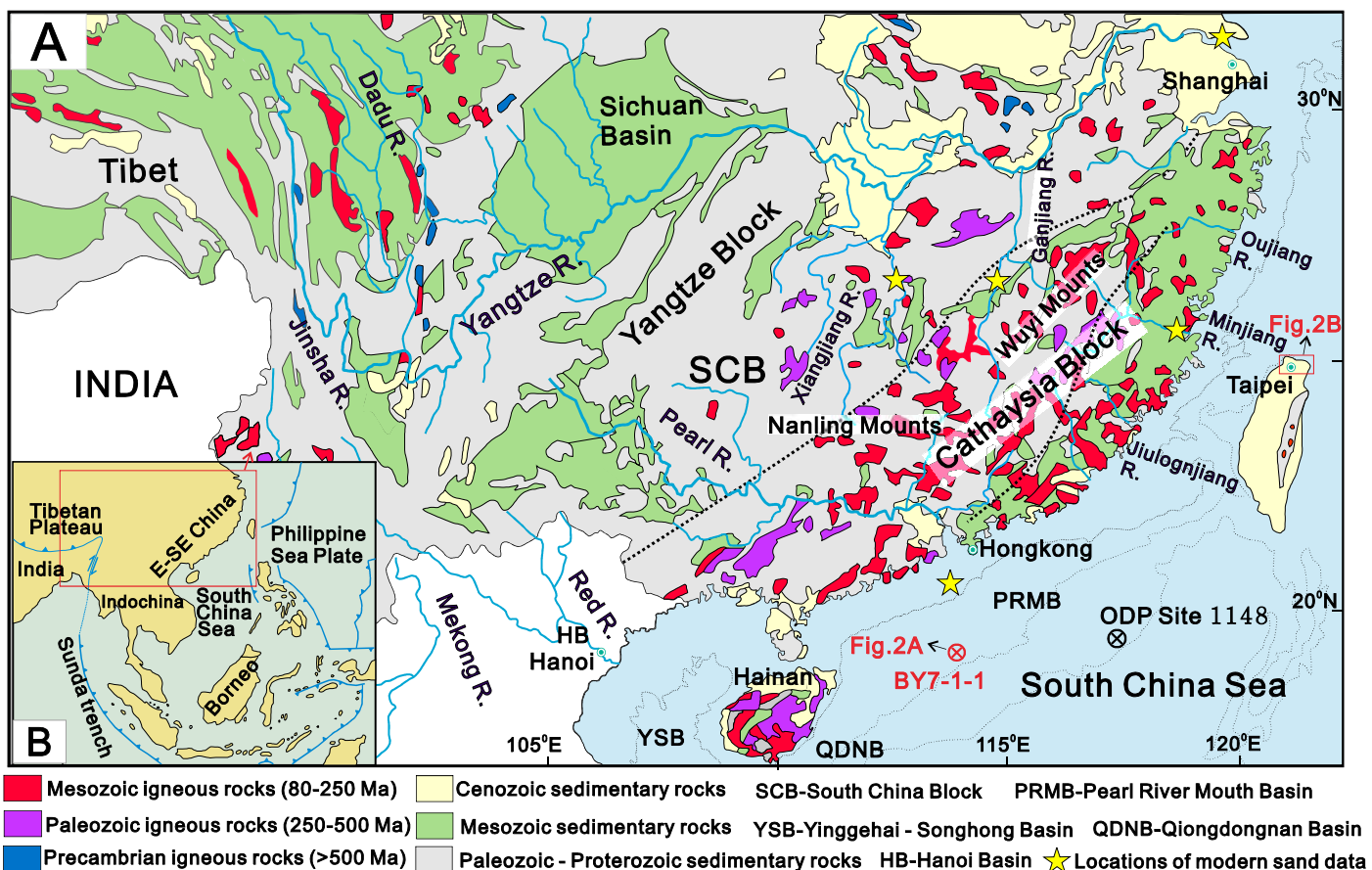
Figure 1. (a) Geological map of E-SE China, showing the spatial-temporal distribution of crystalline basement units and the major fluvial systems. PRMB = Pearl River Mouth Basin; YSB = Yinggehai-Songhong Basin; QDNB = Qiongdongnan Basin; HB = Hanoi Basin. Locations of Well BY7-1-1 and Taiwan samples marked in red. Sample locations from the modern Yangtze, Xiangjiang, Ganjiang, and Minjiang rivers and modern sandstone from the Pearl River Mouth Basin marked by yellow stars. The black dashed lines show the boundary of the Yangtze and Cathaysia Block and northern and southern Cathaysia Block. (b) Simplified tectonic map of East Asia and the environs of the South China Sea.

The stratigraphic and compositional makeup of these accumulated sediments in the South China Sea provide significant information about how the river systems have behaved in tandem with landscape and topographic changes in the eastern Tibetan Plateau during the Late Cenozoic-Quaternary. In addition, lower thermochronometric data have been used to reconstruct the Cenozoic exhumation history of the South China continental margin and eastern margin of Tibet Plateau (Clark et al., 2005; Kirby et al., 2002; Yan et al., 2009). In this paper, we present new stratigraphic, Nd isotope, and U-Pb zircon age data from sediments drilled at Well BY7-1-1 in the Pearl River Mouth Basin (PRMB), as well as from Cenozoic clastic sedimentary sequences exposed in northern Taiwan in order to test the evolving provenance of sediments in the northern margin of the South China Sea. Apatite and zircon fission track dating is carried out in east and southeast Tibet in an attempt to reveal the spatial and temporal linkage between drainage reorganization with the episodic Cenozoic lateral growth of the Tibetan plateau. Comprehensive landscape erosion and sediment archive in the South China Sea is an important way to investigate links between topographic development and drainage system evolution in East Asia.

2. Sedimentary Record in the South China Sea

The continental margin of South China evolved from a dominantly Andean-type active margin during Mesozoic to a Western Pacific-type since Late Cretaceous (Li & Li, 2007). The margin experienced significant extension in the Paleocene that led to the formation of a series of small rift basins, including the Yinggehai-Songhong Basin (YSB), Qiongdongnan Basin (QDNB), and Pearl River Mouth Basin (PRMB) (Ru & Pigott, 1986) (Figure 1).

The sedimentary rocks drilled at Well BY7-1-1 in the South China Sea (Figure 1) are mostly composed of hemipelagic and lacustrine mudstones and sandstones reflecting the rift-drift stage of the South China Sea (Figure 2a). The upper part of the stratigraphic section above the Oligo-Miocene boundary (∼25 Ma) consists of hemipelagic carbonaceous mudstone with interbedded sandstone and siltstone (Qin, 2000). Below this boundary, the section is composed mainly of lacustrine-fluvial sandstone and mudstone. At the boundary are several layers of volcanic tuff that are intercalated with sandstone and mudstone (Figure 2a).

The Cenozoic clastic stratigraphy exposed in northern Taiwan includes synrift and postrift sequences separated by a breakup unconformity dated at 33–39 Ma (Figure 2c; Lan et al., 2014). The postrift sequence consists of argillite and siltstone with abundant shallow-marine fossils. In contrast, the prerift sequence mainly contains conglomerate, sandstone, and siltstone with abundant plant remains, representing a lacustrine and braided river depositional environment (Figure 2c). The Cenozoic sedimentary sequences were uplifted and exposed as a result of arc-continent collision that started after 6.5 Ma (Huang et al., 1997). Therefore, the Cenozoic sedimentary sequences in Taiwan provides an excellent window for gaining insights on the evolution of topography and early river systems in southeast China, especially for the Minjiang River.

A comparative study of the clastic sedimentary sequences in the Pearl River Mouth Basin and northern Taiwan offers potential clues to the sedimentary provenance and drainage evolution in the northern margin of the South China Sea from the east to the west.

3. Sampling and Analytical Methods

3.1. Nd Isotope Analysis

Eighteen mudstone and siltstone core samples collected from the Well BY7-1-1 of the Pearl River Mouth Basin were analyzed for Nd isotope compositions (Figure 2a). The samples were leached with 1 M HCl. Nd isotope compositions were analyzed using a Micromass Isoprobe multicollector mass spectrometer (MC-ICPMS) at the Guangzhou Institute of Geochemistry, Chinese Academy of Sciences, following the procedures in Li et al. (2004). The reported ^{143}Nd/^{144}Nd ratios in this study were adjusted relative to the Shin Etsu JNdi-1 standard of 0.512115. Results are provided in the supporting information Dataset 1.

3.2. Zircon U-Pb Analysis

Seven sandstone core samples collected from the Well BY7-1-1 of the Pearl River Mouth Basin and four sandstones from northern Taiwan were analyzed for zircon U-Pb dating (Figures 2b and 2c). U-Pb ages were measured using a RESOLUTION M-50-LR laser ablation system, coupled to an Agilent7500a ICP-MS based within the Guangzhou Institute of Geochemistry, Chinese Academy of Sciences facilities. External zircon
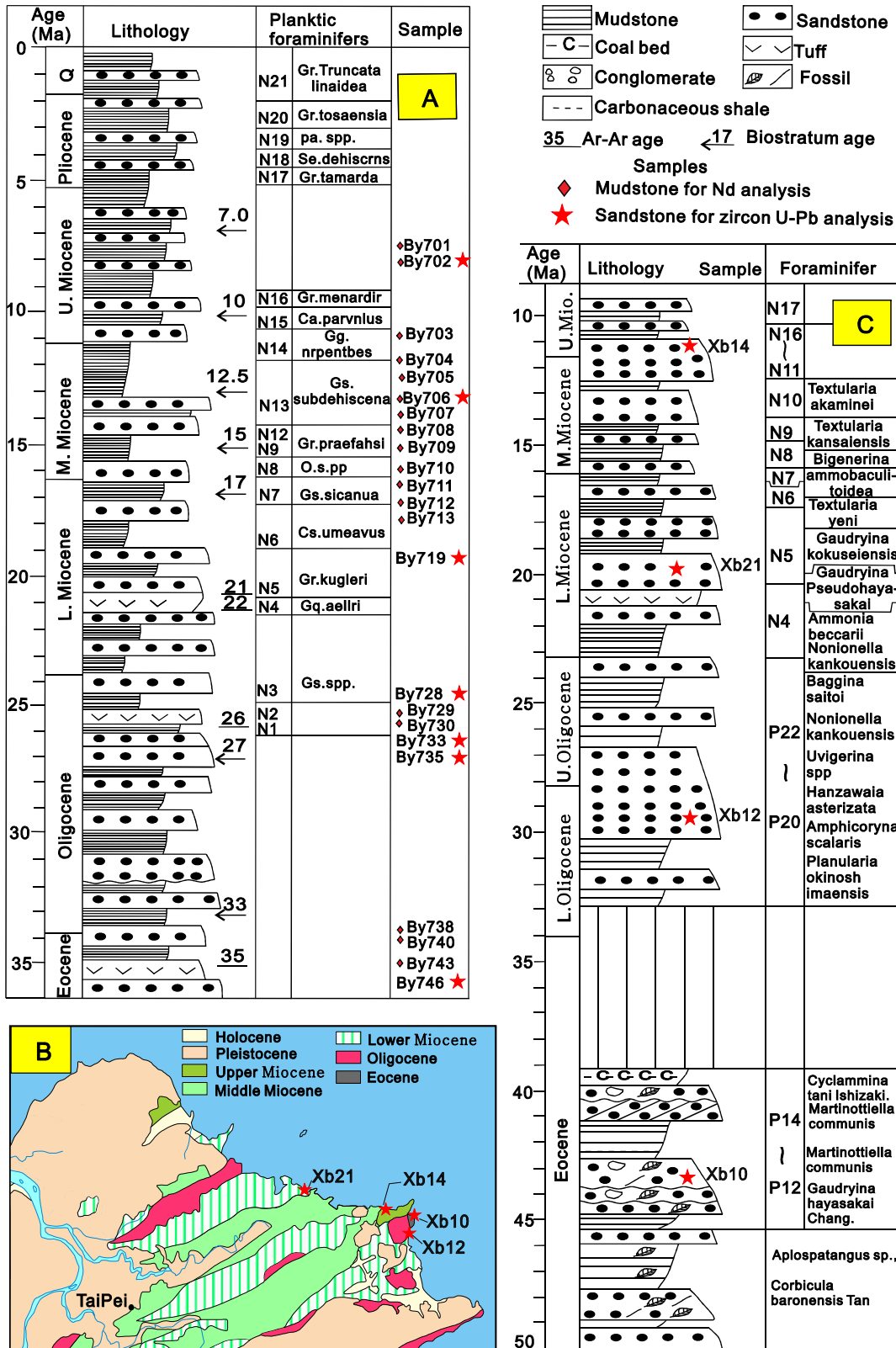
Figure 2. (a) Stratigraphic log of the sedimentary sequences drilled in Well BY7-1-1 of Pearl River Mouth Basin, depicting the major lithological types, their depositional ages, and sample locations. Age constraints are from Qin (2000) and China National Offshore Oil Corporation (CNOOC). (b) Sedimentological map of northern Taiwan, showing the age distribution of Cenozoic clastic rock sequences. Sample locations marked with red stars. (c) Stratigraphic log of the sedimentary sequences in northern Taiwan, depicting the major lithological types, their depositional ages and sample locations. Age constraints are from Huang et al. (2012).

standards Plešovice (TIMS reference age 337.13 ± 0.37 Ma) (Sláma et al., 2008) and TEMORA (TIMS reference age 416.75 ± 0.24 Ma) (Black et al., 2003) were used as the standard. U, Th, and Pb concentrations were calibrated using NIST 610 as reference material (Pearce et al., 1997). Ages were calculated using Isoplot (Ludwig, 2003). Results are provided in the supporting information Datasets 2 and 3.

3.3. Fission Track Analysis

Twenty-two granite samples collected from the eastern margin of Tibet Plateau were analyzed for zircon and apatite fission track dating (supporting information Dataset 4). Sample preparation and fission track analyses were undertaken in the University and Birkbeck College. Glass slides and apatites were etched in 5N HNO_3 at 20°C for 20 s. Zircons were etched using a binary eutectic of potassium hydroxide and sodium hydroxide at 225°C. Etched grain mounts, mica external detectors and corning glass (CN5, CN2, respectively) dosimeters irradiated in the FRM 11 thermal neutron facility at the University of Munich. The external detectors were etched in 48% HF at 20°C for 25 min (Hurford, 1990).

4. Results

4.1. Neodymium Isotopes of Fluvial Sediments

The Nd isotope data from the sedimentary sequence drilled at Well BY7-1-1 show a general uneven decrease in ε_{Nd} values from ~34 to ~11 Ma followed by a subsequent increase (Figure 3c). ε_{Nd} values are higher than −9 for the sedimentary rocks before ~25 Ma but lower than −10 for those clastic units dated at 25–11 Ma (Figure 3c). The ε_{Nd} values of sediments show a slight increase for the ~11 Ma rocks.

4.2. Detrital Zircon Geochronology

Detrital zircon grains of seven samples from Well BY7-1-1 and four samples from northern Taiwan were analyzed for U-Pb geochronology. Between 55 and 197 zircon grains were used for each sample (Figures 4 and 5;
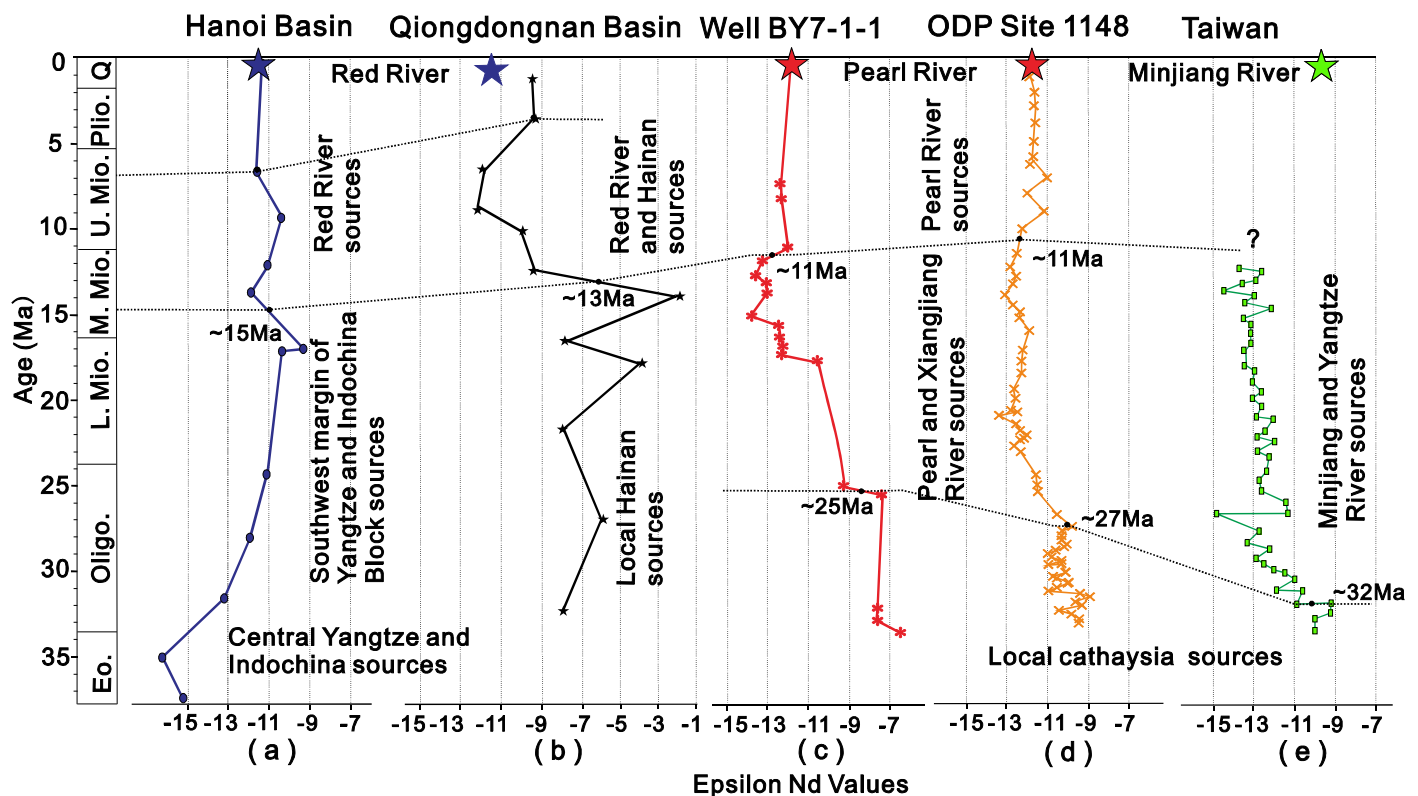
Figure 3. (c) Ranges of Epsilon-Nd values determined for the samples from Well BY7-1-1 of Pearl River Mouth Basin, in comparison to the variations of Epsilon-Nd values documented from sedimentary sequences studied in the (a) Hanoi Basin (Clift et al., 2006a), (b) Qiongdongnan Basin (Yan et al., 2007), (d) ODP Site 1148 (Li et al., 2003), (e) northern Taiwan (Lan et al., 2014) and modern rivers (Clift et al., 2006b; Lan et al., 2014; Li et al., 2003). The present value for CHUR reservoir is $^{143}Nd/^{144}Nd$ = 0.512638, from Hamilton et al. (1983).

Figure 4. Zircon U-Pb age probability density plots of samples from Well BY7-1-1. $^{206}Pb/^{238}U$ used for ages <1,000 Ma, and $^{207}Pb/^{206}Pb$ for older grains. Note the near identical zircon age distribution of Middle-Upper Miocene samples and the modern sands from the Xiangjiang River and the different spectrum from the modern Pearl River. The percentage represents the proportion of young zircon grains (<500 Ma) of the total. Locations of samples shown in Figures 1 and 2. Data of the modern Xiangjiang and Beijiang Rivers are from He et al. (2014) and Xu et al. (2007). Data of the modern sandstone in the Pearl River Mouth Basin are from Zhong et al. (2017).

supporting information Dataset 6). The Eocene to Oligocene samples from Well BY7-1-1 yielded abundant younger grains (<500 Ma), whereas the older zircon grains constitute the more common population in the Miocene stratigraphic units. The Eocene sandstone (By 746) comprised 94% young zircon grains (<500 Ma) with three major age populations at 80–120, 130–170, and 210–260 Ma. Several grains also fall within the age bins of 50–70, 350–450, and 800–1,200 Ma (Figure 4a). The Oligocene samples (By 735, By 733, By 728) have over 87% young zircons (<500 Ma) with age clusters of 80–100, 120–160, 210–260, and 400–500 Ma. The 400–450 Ma age group become a major age peak in the Oligocene and younger stratigraphic units (Figures 4b–4d). The proportion of younger zircons in the Lower Miocene sample (By 719) becomes lower but still shows 76% young zircons (Figure 4e). The zircon U-Pb age populations of Middle-Upper Miocene samples (By 706, By 702) are distinctive in that younger grains fell sharply to 18% and older zircon grains of 700–1,000, 1,100–1,400, 1,700–2,000, and 2,200–2,800 Ma become abundant (Figures 4f and 4g).

The zircon U-Pb age distribution of Eocene to Upper Miocene samples from northern Taiwan shows a similar variation trend with those obtained from Well BY7-1-1 in that the proportion of young zircon grains decreases up section. There are 63% and 59% younger zircon grains in the Eocene and Oligocene samples (Xb 10, Xb 12), respectively, with the major age peaks of 80–180, 200–250, 400–500 Ma and minor ages of 700–1,100 and 1,700–2,000 Ma (Figures 5a and 5b). Neoproterozoic, Paleoproterozoic, and Archean zircon grains constitute major age populations in the Middle-Upper Miocene samples (Xb 21, Xb 14) with age clusters of 700–1,100, 1,500–2,000, and 2,200–2,500 Ma. The percent of young zircons in the Lower Miocene sample is 39% and drops to 30% in the Upper Miocene samples with the major age peaks of 80–180, 200–270, and 350–500 Ma (Figures 5c and 5d).

4.3. Fission Track Chronology
Two samples from the margin adjacent to western part of the Sichuan Basin yield zircon fission track (ZFT) ages of 61.9 ± 2.9 and 69 ± 2.8 Ma and eight apatite fission track (AFT) central ages range from 6.9 ± 1.1 to 3.2 ± 1.1 Ma (Figure 6 and supporting information Dataset 4).

ZFT central ages of three samples from the Diancangshan Mountains are 7.5 ± 0.7, 8.3 ± 0.4, and 6.0 ± 1.3 Ma, respectively, while AFT central ages range from 1.4 ± 0.3 to 6.8 ± 0.6 Ma. In contrast, AFT central ages of the samples from the Panzhihua area and Jianchuan Basin are relative old from 27.8 ± 2.0 to 53.5 ± 5.2 Ma (Figure 6). These samples show continued cooling since about 50 Ma (Figure 7).

5. Discussion

5.1. Implications for Provenance in the South China Sea
5.1.1. Local Marginal Sources Before ~25 Ma
Although the variation trend of ε_{Nd} values at Well BY7-1-1 is consistent with the data obtained from ODP Site 1148 and the Cenozoic clastic sequence in northern Taiwan, the ε_{Nd} values obtained from ~25 Ma and older sediments in Well BY7-1-1 are less negative than that from ODP Site 1148 (Li et al., 2003) and northern Taiwan (Lan et al., 2014) (Figures 3d and 3e). The relatively high ε_{Nd} values most likely reflects more influx from intermediate to silicic igneous sources to Well BY7-1-1 (Li et al., 2003). Several thin volcanic layers have been identified in Well BY7-1-1 (Figure 2a) (Qin, 2000).

The ε_{Nd} values of pre-25 Ma sediments from Well BY7-1-1 and ODP Site 1148 and pre-31 Ma from northern Taiwan are much less negative than those measured from modern sediments in the Pearl River (average $\varepsilon_{Nd} = -11.8$; Li et al., 2003) and the Yangtze River (average $\varepsilon_{Nd} = -13$; Yang et al., 2007). Higher Nd isotope data and abundant younger detrital zircon ages of the Eocene-Oligocene sedimentary rocks from the Pearl River Mouth Basin and northern Taiwan suggest that the Phanerozoic igneous rocks in the coastal region of Cathaysia contributed much of the sediments to the South China Sea during the early stages of its rift-drift tectonics (Figures 8c, 8d, 9d, and 9e).

Several magmatic events have been identified in the Cathaysia Block, including Caledonian (500–400 Ma), Hercynian-Indosinian (250– 200 Ma) and Yanshannian (190–80 Ma) igneous pulses. Early Paleozoic granitoids (400–450 Ma) and Permo-Triassic granitic plutons (260–210 Ma) are abundant along the northern boundary of Cathaysia and in the interior parts of the Yangtze Block (Chen & Jahn, 1998; Li & Li, 2007) (Figure 1). Late Mesozoic (Yanshanian) magmatic rocks are exposed widely with a coastward-younging trend (Li, 2000) (Figures 1 and 9a). Early Cenozoic magmatism, including the 60–17 Ma bimodal volcanism and ca.

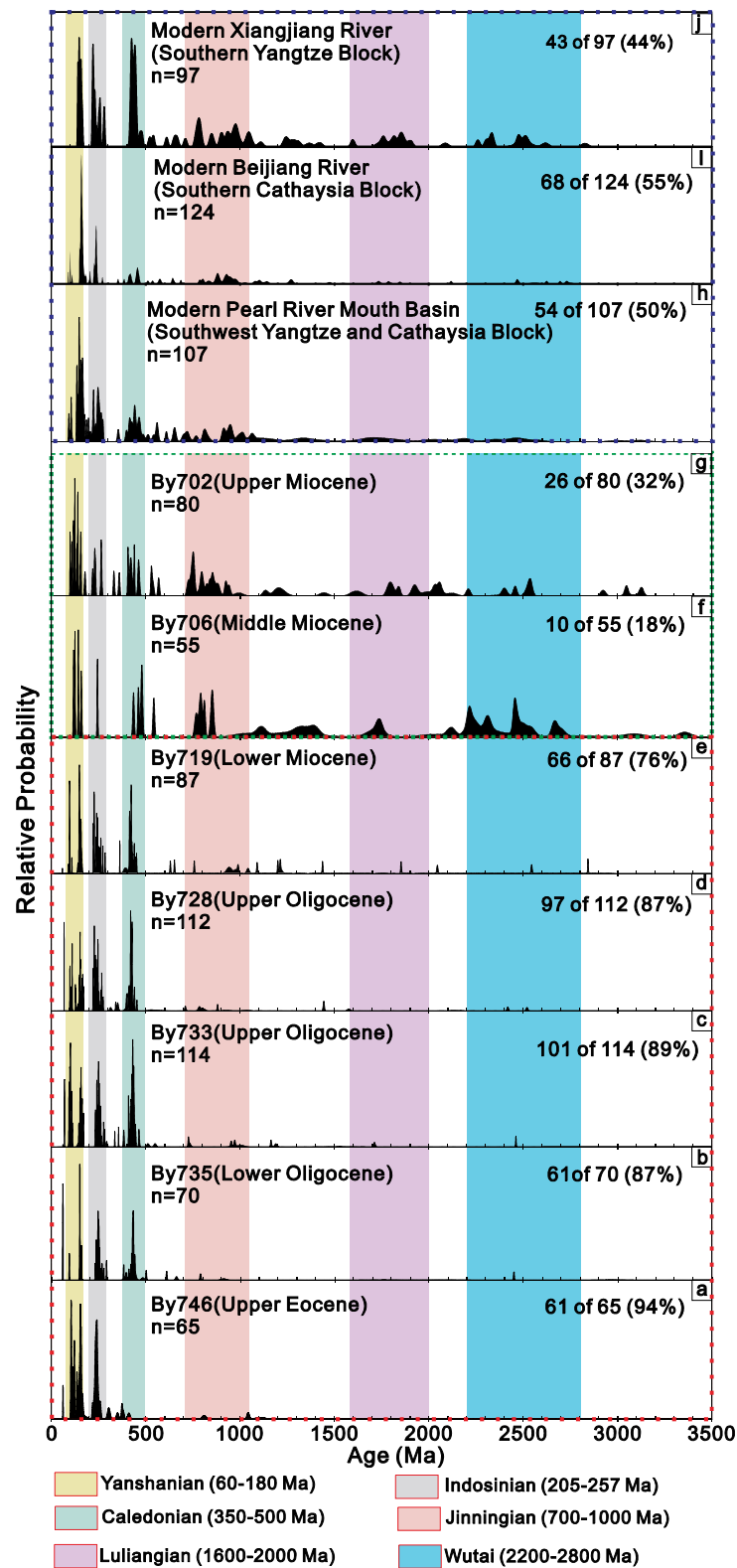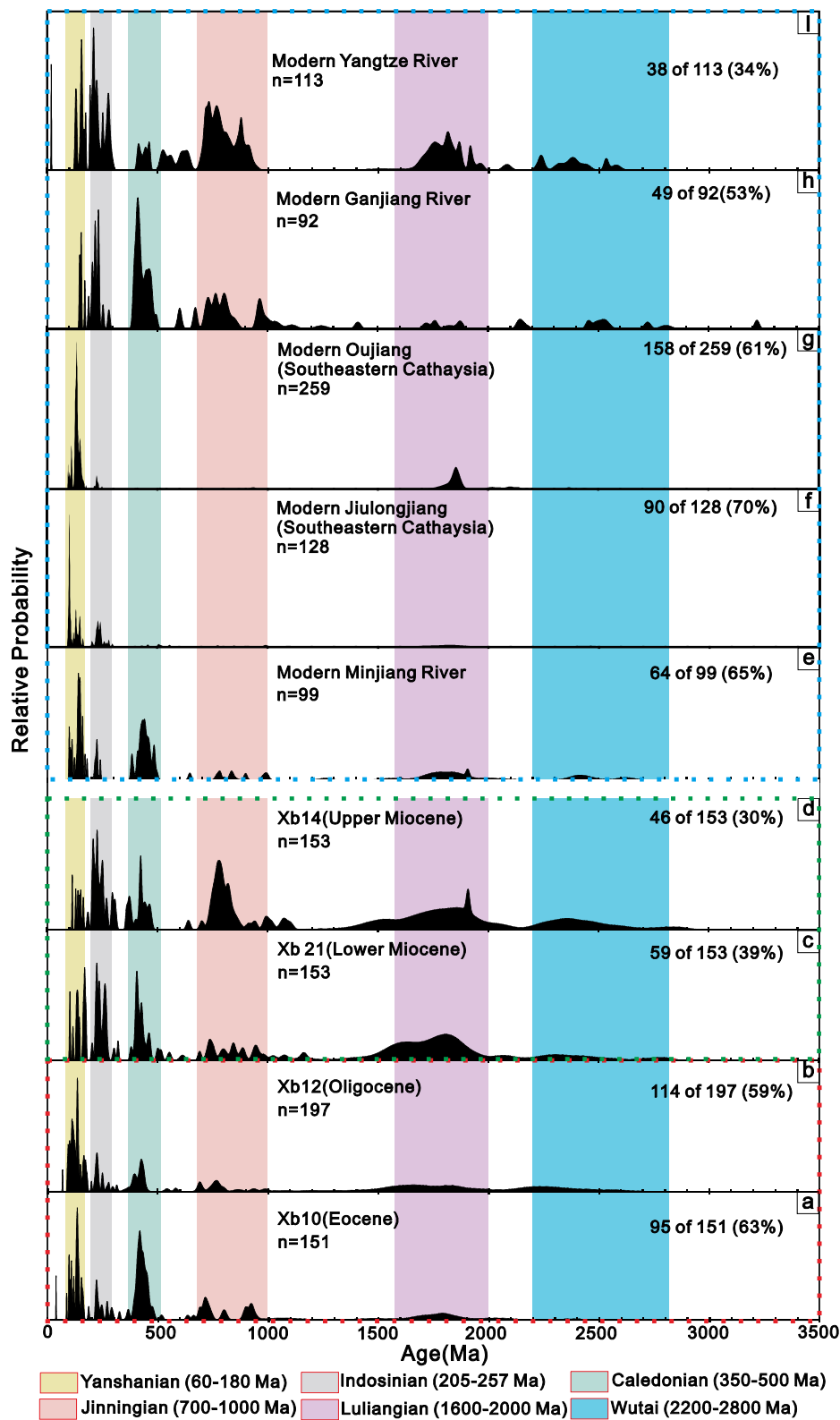**Figure 5.** Zircon U-Pb age probability density plots of samples from northern Taiwan. $^{206}Pb/^{238}U$ used for ages < 1,000 Ma, and $^{207}Pb/^{206}Pb$ for older grains. Note the near identical zircon age distribution of Middle-Upper Miocene samples and the modern sands from the Yangtze River and the different spectrum from the modern Minjiang River. The percentage represents the proportion of young zircon grains (<500 Ma) of the total. Locations of samples shown in Figures 1 and 2. Data from the modern Yangtze and Ganjiang River is from He et al. (2014). Data from the modern Minjiang River is from Zhang et al. (2017).

Figure 6. Topographic map together with measured fission track ages from the eastern Tibetan Plateau.

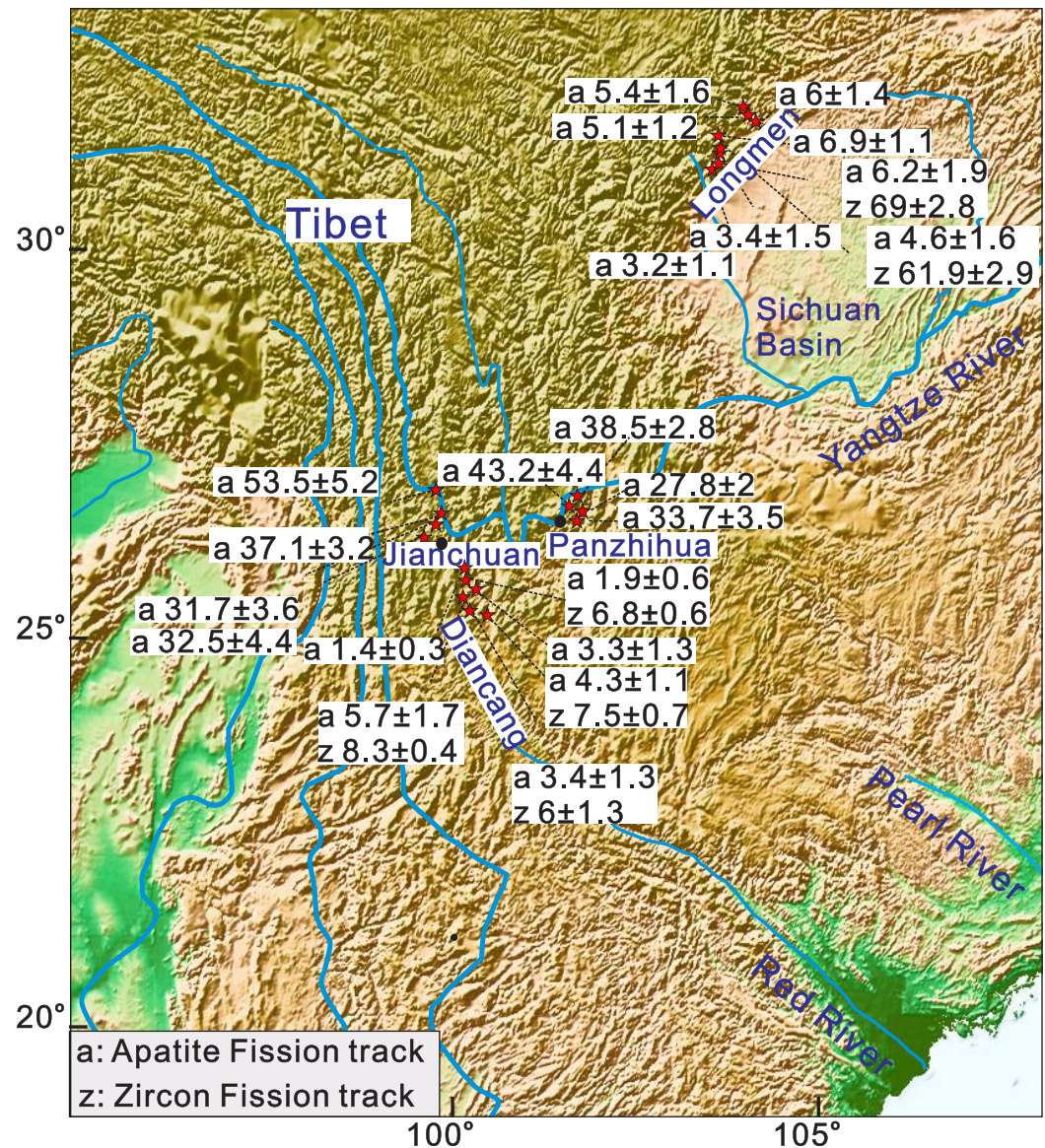60–6 Ma rift magmatism occurred in the small basins (Chung et al., 1997; Zhou et al., 2009) and the Taiwan Strait (Lin et al., 2003). These igneous rocks with ε_{Nd} values ranging from −10 to −5 also show roughly NW to SE general increasing trends both in the Yangtze and Cathaysia blocks although there is considerable overlap (Figure 8a).

Comparison of the Nd isotopes of sediments from major rivers flowing into the South China Sea, Li et al. (2003) suggests that pre-27 Ma sediments were dominantly derived from a southwestern provenance (Indochina-Sunda Shelf and possibly northwestern Borneo). In fact, the detritus from Borneo to the northern margin of the South China Sea are impossible as the Proto-South China Sea would cut off any connection between the northern margin of the South China Sea and Borneo at that time. Although Cretaceous granites are also exposed in the Indochina, these Cretaceous granites are intrusive into Precambrian metamorphic rocks and Paleozoic granites (Usuki et al., 2013). In addition, Triassic granites are more abundant than Cretaceous granites in the Indochina-Sunda Shelf (Carter et al., 2001), but very few Precambrian and less Triassic detrital zircons have been reported from the Eocene-Oligocene sandstones of the Pearl River Mouth Basin and northern Taiwan (Figures 4 and 5).
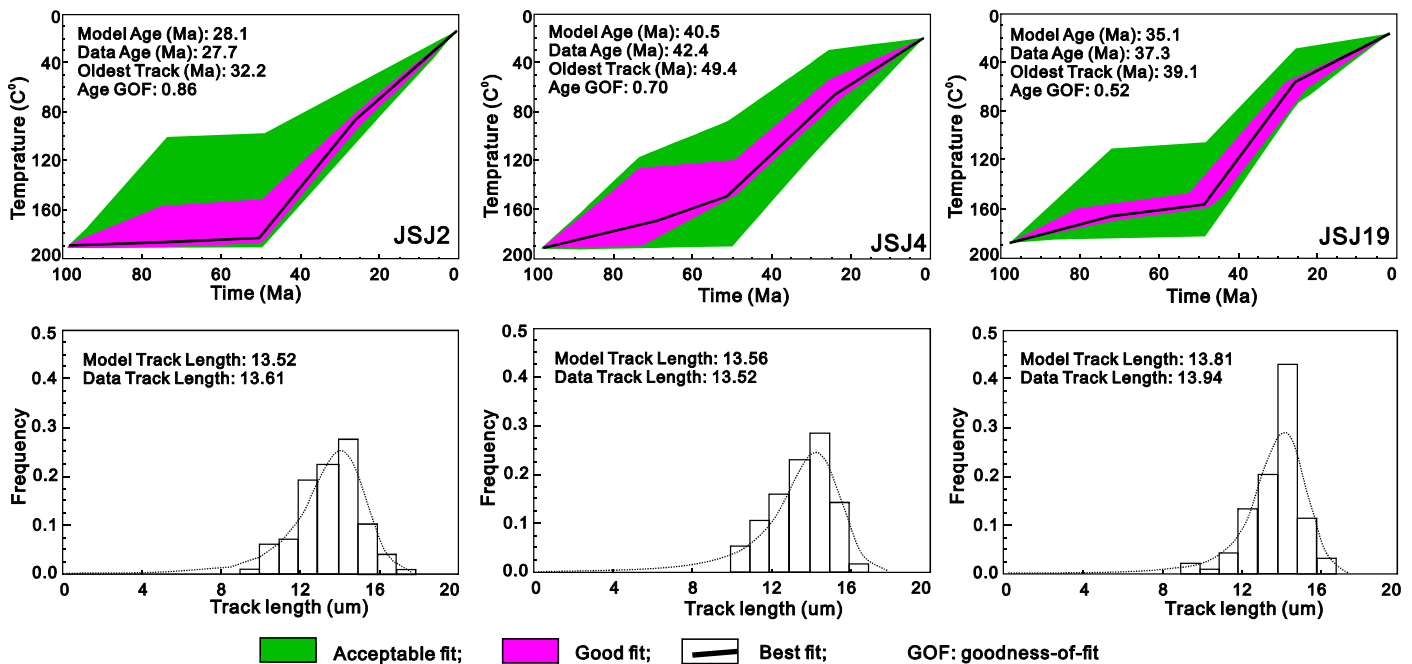
Figure 7. Representative plots of fission track modeled thermal histories from the eastern Tibetan Plateau.

In the northwestern part of the South China Sea, the ε_{Nd} values of sediments from the Qiongdongnan Basin do not show obvious decreasing trend until ∼13 Ma (Figure 3b; Yan et al., 2007). The zircon U-Pb results are dominated by age population at 100–300 Ma, which do not correlate with the age pattern of sediments in the currently drainage of the Red River (Figure 9c; Hoang et al., 2009; Yan et al., 2011b). The higher ε_{Nd} values and younger zircon ages of the Oligocene-Middle Miocene sediments mainly reflect a major contribution from local plutonic rocks, especially from the Hainan Island (Yan et al., 2011b). In contrast, the strongly negative ε_{Nd} values of the sediments before ∼25 Ma in the Hanoi Basin are consistent with erosion from ancient Yangtze Block (Figure 8b; Clift et al., 2006a). The substantial difference between the sediments from the Hanoi Basin and the Qiongdongnan Basin indicates that the detritus carried by the Red River did not reach the Qiongdongnan Basin, but were mainly trapped in the Hanoi Basin and in the northwest of the Yinggehai-SongHong Basin before ∼25 Ma.

5.1.2. Continental Interior Sources Since ∼25–11 Ma

The Nd isotopic compositions of 25–11 Ma sediments from Well BY7-1-1 and ODP Site 1148 and northern Taiwan decrease and show values slightly more negative than that of the modern sediments from the Pearl River (Hu et al., 2013; Li et al., 2003) and the Minjiang River (Figures 3c, 3d, and 3e; Lan et al., 2014). At the same time, Early Paleozoic (400–450 Ma) detrital zircons make up a major population in the Oligocene strata drilled at Well BY7-1-1. Proterozoic and Archean zircons comprise major age populations in the Middle-Upper Miocene samples (Figure 4).

The South China Block composed of Yangtze Block to the northwest and Cathaysia Block to the southeast (Figure 1). The basement of the Yangtze Block is composed of Archean and Paleoproterozoic rocks, with average ages in the range of 2,700–2,800 and 2,200–2,500 Ma, whereas the Cathaysia Block is composed dominantly of Paleo to Mesoproterozoic units, with some Late Achaean rocks (∼2,500 Ma) (Chen & Jahn, 1998). Paleoproterozoic (1,800–2,000 Ma) detrital zircons are also abundant in the Paleozoic and Mesozoic strata in northern Cathaysia and in the central Yangtze Block (Yan et al., 2011a).

Lower Nd isotopic values and more Proterozoic and Archean zircons in the Miocene samples indicate that northern Cathaysia and/or the Yangtze Block started to supply more sediments to the South China Sea. The provenance transition can be examined using the Multidimensional Scalar (MDS) statistical analysis of Vermeesch et al. (2016). In the MDS plot (Figure 10), the Eocene-Oligocene samples and the Miocene samples from Well BY7-1-1 and northern Taiwan are divided into two clear groups obviously. The Eocene-Oligocene
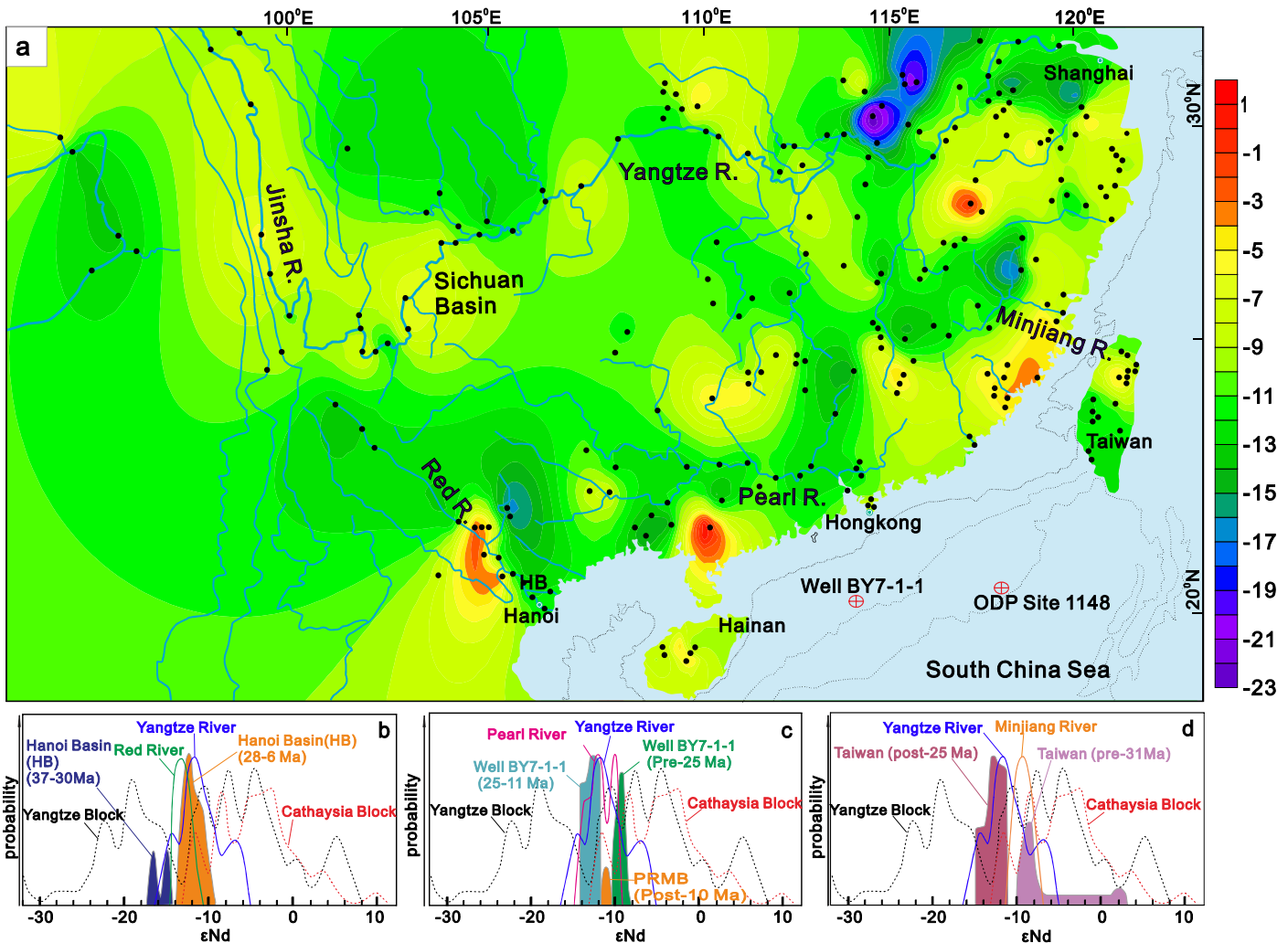
Figure 8. (a) Contoured map of εNd (0) values for sedimentary rocks, granitic intrusions, acid volcanic rocks and modern sediments from the South China Block and eastern Tibetan Plateau. (b) Relative probability plots of Nd isotopic compositional ranges of possible source terrains, major river drainage systems and the samples from Hanoi Basin, (c) Well BY7-1-1 and (d) northern Taiwan. Nd values of source terrains and rivers are from Darbyshire & Sewell (1997), Chen and Jahn (1998), Liu et al. (2007), Shao et al. (2009, 2014), Goldstein et al. (1984), Li et al. (2003), Lan et al. (2000), Gilder et al. (1996), Lan et al. (2014), Yang et al. (2007), Yan et al. (2007), Fang et al. (1992), Wu et al. (2010), Zhang et al. (2007), Ma et al. (1997), Li and Ma (1991), Ma et al. (2000), Meng et al. (2008), and Clift et al. (2004). The references and data are also provided in supporting information Dataset 5.

samples lie closer to the Beijiang and Jiulongjiang, respectively, while the Miocene samples lie closer to the Xiangjiang and Yangtze River.

The ε_{Nd} values in the Hanoi Basin demonstrate an opposite trend to the ε_{Nd} values from the Pearl River Mouth Basin and northern Taiwan towards less negative since ca. 35 Ma (Figure 3a). Strongly negative ε_{Nd} values for pre-25 Ma sedimentary rocks depart obviously from those of the modern sediments in the Red River but have been with error of the modern values since ∼25 Ma (Figure 3a and supporting information Dataset 5) (Clift et al., 2006a). Several samples deposited at 15–10 Ma are somewhat even less negative in ε_{Nd} values than the modern sediments in the Red River (Clift et al., 2006a). The ε_{Nd} values and zircon U-Pb age distribution patterns of the post-25 Ma sediments are similar to the modern sediments in the Red River, indicating that the contributions from the Yangtze Block become less (Hoang et al., 2009; Yan et al., 2011b; Zhao et al., 2015b).

5.1.3. Eastern Margin of the Tibetan Plateau Sources Since ∼11 Ma

The ε_{Nd} values of sediments in Well BY7-1-1 and ODP Site 1148 younger than ∼11 Ma show an increase to −11.5 again. Compared with the detrital zircon age distribution in the Miocene samples from the Pearl River Mouth Basin, Proterozoic, and Archean zircons are rare in the Quaternary sand deposits of the Pearl River
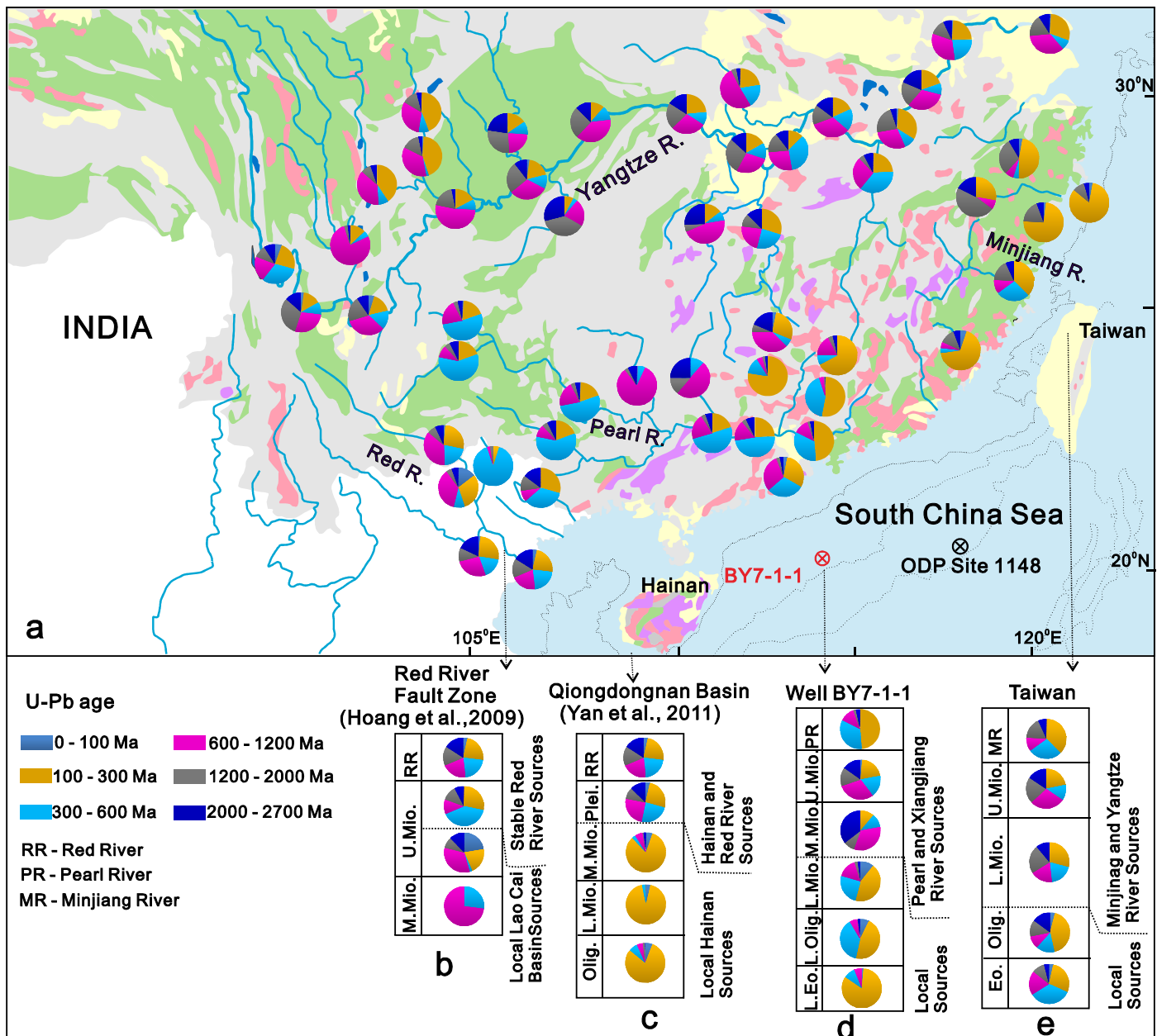
Figure 9. (a) Detrital zircon ages of the major source areas (Clift et al., 2006a; He et al., 2014; Hoang et al., 2009; Xu & Chen, 2010; Xu et al., 2007; Zhao et al., 2015a; supporting information Dataset 6 and references therein), as compared with those from sediment samples of the (b) Red River Fault Zone (Hoang et al., 2009), (c) Qiongdongnan Basin (Yan et al., 2011b), (d) Well BY7-1-1, and (e) northern Taiwan.

Mouth Basin (Figures 3c, 3d, and 4). We, therefore, infer that some of the detritus supply to the Pearl River Mouth Basin from northern Cathaysia and/or the Yangtze Block was switched off by ~11 Ma.

Furthermore, we note a marked shift in ε_{Nd} values of sediments from the Qiongdongnan Basin during the Late Miocene (Figure 3b). Sedimentary ε_{Nd} values from the Qiongdongnan Basin are also less negative than those from ODP Site 1148 and northern Taiwan, but do not show decreasing trend until ~13 Ma (Figure 3b) (Yan et al., 2007). The ε_{Nd} values are higher than −8 for pre-13 Ma sedimentary rocks and lower for post-13 Ma sedimentary rocks. The zircon U-Pb age data are dominated by age peaks at 100–300 Ma for the lower member of the Upper Miocene, but show more older grains (>300 Ma) for the Pleistocene (Figure 9c; Wang et al., 2015). The ε_{Nd} values and zircon U-Pb age pattern show a change from local sources to more erosion from the eastern margin of Tibetan Plateau sources, mostly from the southern Yangtze Block and Indochina
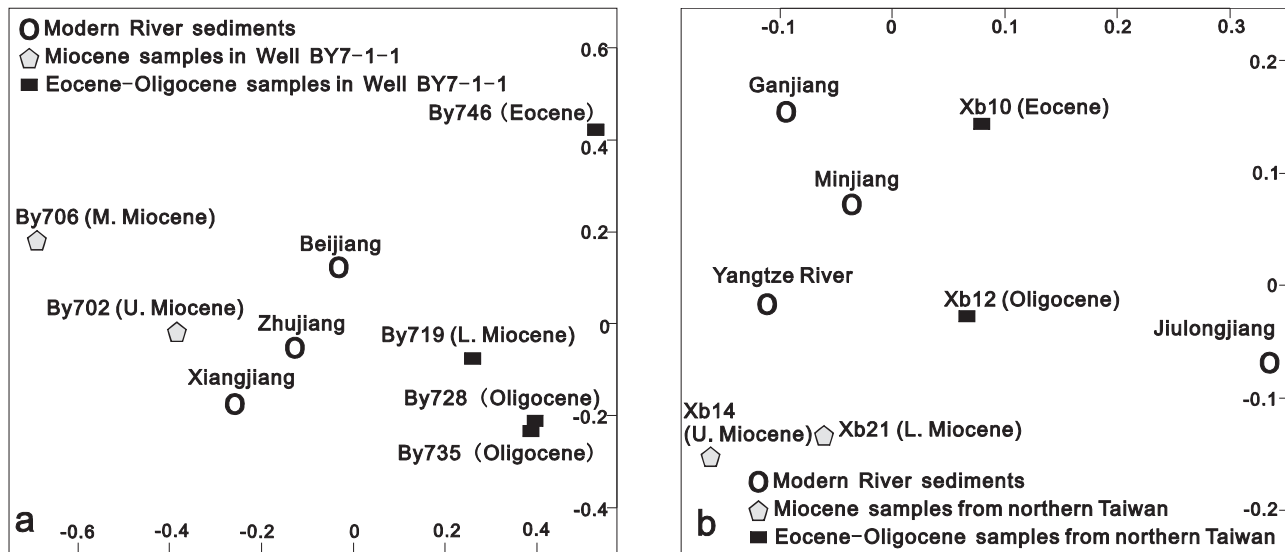
Figure 10. Nonmetric multidimensional scaling map of U-Pb ages of the samples from Well BY7-1-1 and northern Taiwan and the modern river sediments.

to the west of the South China Sea. The detritus carried by the Red River started to reach the southeastern part of the Yinggehai-SongHong Basin and even up to the central part of the Qiongdongnan Basin since the Late Miocene.

5.2. River Drainage Reorganization in Cenozoic East Asia
5.2.1. First River Drainage Reorganization Since ~25 Ma

Detrital sediments derived from the eastern margin of the Tibetan Plateau and southern China are delivered to the northern part of the South China Sea by three large river systems at present: the Red, Pearl, and Minjiang Rivers (Figure 1). The eroded rock volumes for drainage areas similar in scale to the present-day Dongjiang and Beijiang Rivers are 7×10^3 and 114.8×10^3 km^3, respectively (Table 1). The balance between the estimated volumes of eroded rock from the Dongjiang and Beijiang Rivers and sediment volumes in the Pearl River Mouth Basin before the opening of the South China Sea (45–30 Ma) indicates that the local bedrocks contributed much of the sediments to the South China Sea (Figures 11a and 12; Table 1). Phanerozoic igneous rocks exposed in SE China contributed most sediment flux to this depocenter presumabably via small local rivers (Figure 12a). Some eroded materials must have been trapped in the small rift basins along the southeast margin of the South China Block, such as the Sanshui Basin (SSB). The eroded rock volumes

Table 1

Comparison of Sediment Rock Volumes in the Pearl River Mouth Basin With Maximum Volumes of Erosion for Drainage Areas Similar in Scale to the Present-Day Based on Thermal History Models of Apatite Fission Track and (U-Th)/He Data (Yan et al., 2009)

Pearl River Mouth Basin, Stratum Age	Total sediment rock volume in basin (km^3)	Porosity	Loss due to chemical weathering	Corrected total eroded rock volume (km^3)	Maximum volume of erosion indicated by cooling histories of bedrock (km^3)		Need contributions from Xijiang branch (km^3)
					Dongjiang (35×10^3 km^2)	Beijiang (47×10^3 km^2)	Xijiang (304×10^3 km^2)
0–10 Ma	85×10^3	30%	10%	65.4×10^3	14×10^3	18.8×10^3	32.6×10^3
30–10 Ma	270×10^3	20%	10%	237.6×10^3	21×10^3	37.6×10^3	179×10^3
45–30 Ma	75×10^3	15%	10%	70.1×10^3	7×10^3	114.8×10^3	0

Note. Results from thermal history modeling show all of the samples in the southern margin of the South China Block experienced a similar style of thermal history composed of three distinct stages: (1) rapid cooling in the early Cenozoic that differs in timing from the south to the north, (2) 20–40 Myrs of relative stasis at ~70–60°C; (3) rapid cooling to surface temperatures that initiated between 15 and 10 Ma. The denuded thickness is calculated based on the modeled thermal histories and average geothermal gradient value of 30°C/1,000 m. Sediment volumes for the Pearl River Mouth Basin are from Clift et al. (2006a). To enable direct comparison with bedrock erosion the basin volume data have also been adjusted for loss due to chemical assumed to 10% and corrected for sediment porosity.
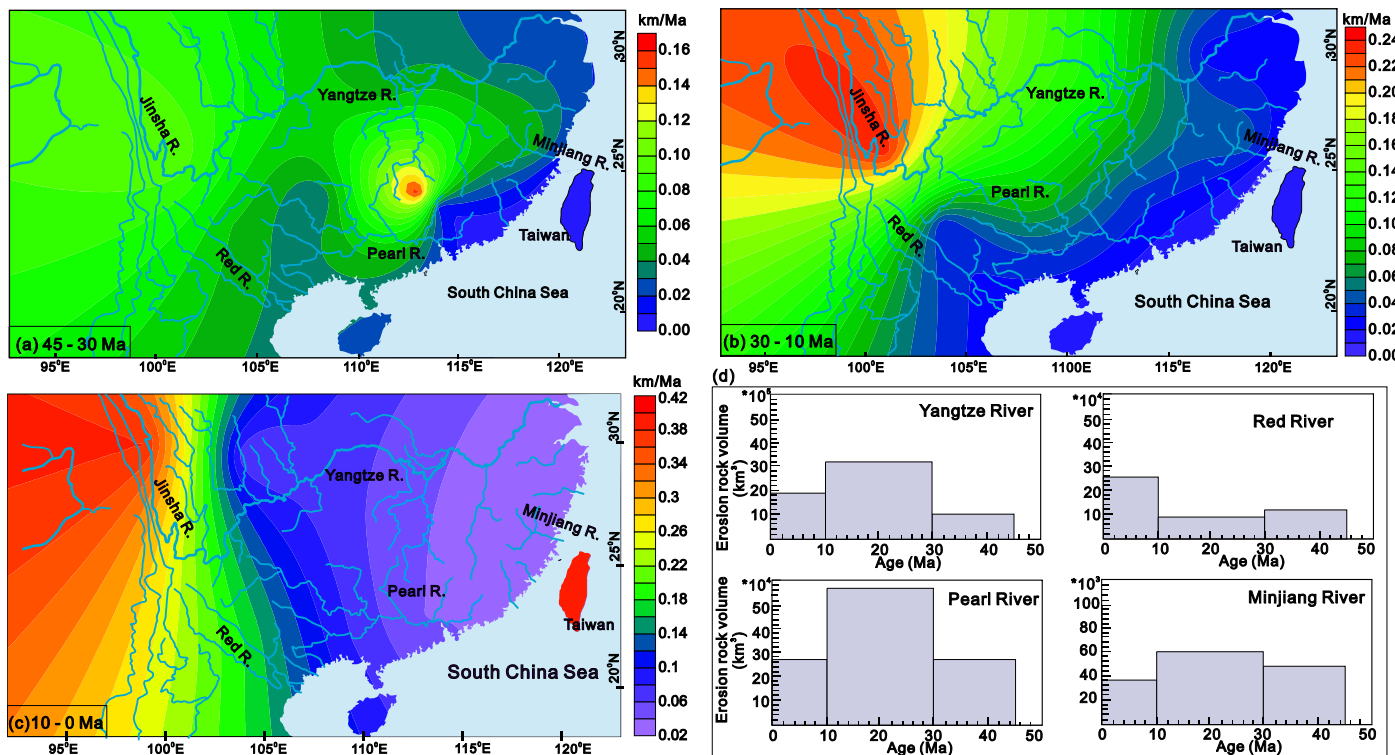
Figure 11. (a–c) Erosion of the eastern Tibetan Plateau and the South China Block based on thermal history models of apatite fission track and (U-Th)/He data (An et al., 2008; Beyssac et al., 2007; Clark et al., 2005; Godard et al., 2009; Hsu et al., 2016; Kirby et al., 2002; Lei et al., 2006, 2008; Li et al., 2005; Liao et al., 2005; Maluski et al., 2001; Richardson et al., 2010; Shi et al., 2006, 2011; Viola & Anczkiewicz, 2008; Wan et al., 1997; Wang et al., 1994, 2012; Wu et al., 2002; Yan et al., 2009, 2011a; Zhou et al., 2003, 2005; supporting information Dataset 7 and references therein). (d) Erosion rock volumes from major river drainage systems.

for drainage areas similar in scale to the present-day Minjiang and Pearl River before the opening of the South China Sea (45–30 Ma) are 48×10^3 and 273.8×10^3 km^3, respectively (Figure 11d and Table 2). The eroded rock volumes calculated by the thermal history models of apatite fission track and (U-Th)/He data for drainage areas similar in scale to the present-day Yangtze and Red River are 114×10^3 and 998×10^3 km^3, respectively (Figure 11d and Table 2). Part of this mass must have been transported southwest into the Paleo-South China Sea (Hoang et al., 2009).

Increased detrital flux to the South China Sea during the Middle-Late Miocene from the sources in northern Cathaysia and even possibly from center of the Yangtze Block suggests significant headwater propagation of the Pearl River drainage system into the continental interior (Figure 12b). The Nd isotopic compositions of 15–11 Ma sediments from Well BY7-1-1 and ODP Site 1148 show values more negative than that of the modern sediments in the Pearl River. We infer that the headwaters of the Pearl River possibly have drained parts of the Yangtze Block in what is now the Lower Yangtze River fluvial basin (e.g., Xiangjiang) in the Middle-Late Miocene. The Mesoproterozoic age cluster (1,000–1,400 Ma) in the Middle-Upper Miocene samples are absent in the modern sediments from the Pearl River but can be found in the Xiangjiang River (Figures 4h, 4l, and 4j). The volume of eroded rock between 30 and 10 Ma from Dongjiang and Beijiang catchment is much less than that deposited in the Pearl River Mouth Basin (Table 1), implying that the Xijiang and/or Xiangjiang Rivers must have contributed substantial sediments to the Pearl River Mouth Basin (Figure 12b).

Lower ε_{Nd} values and more Proterozoic and Archean zircon grains of 25–11 Ma sediments from northern Taiwan than those of modern sediments in the Minjiang River suggest that northern Cathaysia and/or the Yangtze Block supplied most of the sediment to northern Taiwan in the Miocene. However, the mechanism of transport of the sediments in the Yangtze Block and/or northern Cathaysia to northern Taiwan remains unclear. One possible explanation is that the headwaters of the modern Minjiang River propagated northward and reached up to the Lower Yangtze River fluvial basin (e.g., Ganjiang River; Lan et al., 2014).
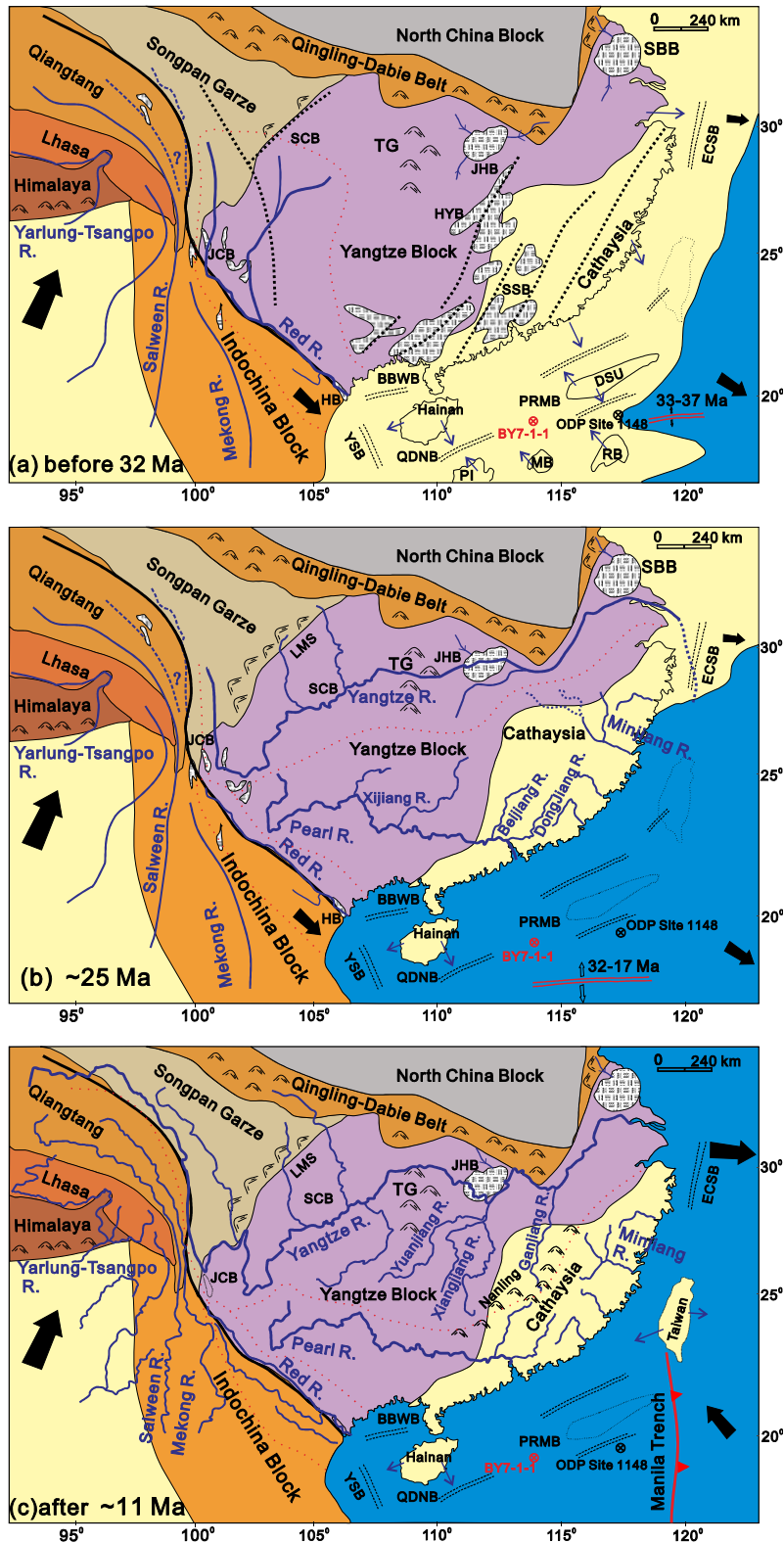
Figure 12. Simplified maps showing the provenance of the South China Sea and evolution of the regional drainage systems. Black arrows show stress direction. Black dashed line shows main faults. Black dashed double-line show rifting center. Red dashed line show assumption watershed lines. PRMB = Pearl River Mouth Basin; QDNB = Qiongdongnan Basin; YSB = Yinggehai-Songhong Basin; BBWB = Beibuwan Basin; HB = Hanoi Basin; JHB = Jianghan Basin; JCB = Jianchuan Basin; SCB = Sichuan Basin; SBB = Subei Basin; ECSB = East China Sea Basin; HYB = Hengyang Basin; SSB = Sanshui Basin; LMS = Longmenshan Mountains; TG = Three Gorges; DSU = Dongsha Uplift; PI = Parace (Xisha) Island; MB = Macclesfield (Zhongsha) Bank; RB = Reed (Liyue) Bank.

Table 2
The Eroded Rock Volumes for Drainage Areas Similar in Scale to the Present Minjiang, Pearl, and Yangtze Rivers

	Yangtze River			Pearl River				
Drainage Branch area (km^2)	Upper Yangtze 340 × 10^3	Middle Yangtze 680 × 10^3	Lower Yangtze 200 × 10^3	Dongjiang 35 × 10^3	Beijiang 47 × 10^3	Xijiang 304 × 10^3	Red River 143 × 10^3	Minjiang River 60 × 10^3
Erosion volume (km^3)								
0–10 Ma	1,292 × 10^3	544 × 10^3	60 × 10^3	14 × 10^3	18.8 × 10^3	243 × 10^3	257 × 10^3	36 × 10^3
Total	**1,896 × 10^3**			**275.8 × 10^3**			**257 × 10^3**	**36 × 10^3**
30-10 Ma	1,598 × 10^3	1,496 × 10^3	100 × 10^3	21 × 10^3	37.6 × 10^3	516*10^3	85 × 10^3	60 × 10^3
Total	**3,194 × 10^3**			**574.6 × 10^3**			**85 × 10^3**	**60 × 10^3**
45-30 Ma	510 × 10^3	408 × 10^3	80 × 10^3	7 × 10^3	114.8 × 10^3	152 × 10^3	114 × 10^3	48 × 10^3
Total	**998 × 10^3**			**273.8 × 10^3**			**114 × 10^3**	**48 × 10^3**

Note. The denuded thickness of the Minjiang, Pearl, and Yangtze Rivers is calculated based on the modeled thermal histories of the bedrock and average geothermal gradient value of 30°C/1,000 m. The modeled results of the Upper Yangtze River are from Clark et al. (2005) and this study. The modeled results of the Middle Yangtze River are from Kirby et al. (2002), Wang et al. (2012), and Richardson et al. (2010). The modeled results of the Lower Yangtze River are from Zhou et al. (2003). The modeled results of the Dongjiang and Beijiang Rivers are from Yan et al. (2009). The modeled results of the Xijiang River are from Li et al. (2005). The modeled results of the Red River are from Maluski et al. (2001) and Lei et al. (2006, 2008). The modeled results of the Minjiang River are from Wang et al. (1994).

Alternately, the materials in the Yangtze Block and/or northern Cathaysia were transported to the East China Sea by the Yangtze River, further southward reaching the middle of the Taiwan Strait (Zhang et al., 2017). The interpretation that materials in the Yangtze Block and/or northern Cathaysia were transported from north to south is consistent with the paleogeographic reconstructions based on the Middle Miocene lithofacies distribution in the region, suggesting higher surface elevation to the north and deep marine environment in the South China Sea to the SE, as well as lacustrine and fluvial deposition in the northern part of the East China Sea to the NE (Li et al., 2010).

The sedimentary record from the Hanoi Basin and the Lower Yangtze close to the delta corroborates an important inferred river—capture event and that the Middle Yangtze was lost to the Yangtze River by Early Miocene (Clift et al., 2006a; Zhang et al., 2017; Zheng et al., 2013). The drainage reversal in the central Yangtze basin was consistent with the fast erosion of the SE margin of Tibet since ∼25 Ma (Figure 11b). The eroded rock volumes for drainage areas similar in scale to the present Minjiang, Pearl, and Yangtze Rivers increased to 60 × 10^3, 574.6 × 10^3, and 3194 × 10^3 km^3, respectively (Figure 11d and Table 2).Voluminous materials eroded from the Tibetan Plateau and South China Block accumulated within the East China and South China Seas during Miocene (Figure 11b).

5.2.2. Second River Drainage Reorganization Since ∼11 Ma
Much of the detrital supply to the South China Sea from parts of northern Cathaysia and possibly from the Yangtze Block was switched off by ∼11 Ma, reflecting another phase of changes in the erosion pattern and drainage divide migration in the Pearl River or Minjiang drainage system. The drainage divide between the Pearl River drainage and the Lower Yangtze River drainage migrated southward, possibly in response to the Late Miocene uplift of the eastern Tibetan Plateau to the W-NW (Clark et al., 2005; Kirby et al., 2002) and of southern China to the E-SE (Yan et al., 2009) (Figure 11c). The ε_{Nd} values of the post-∼11 Ma sediments are similar to the modern sediments in the Pearl River Delta, indicating that the Pearl River drainage has been similar to the modern fluvial system (Figure 12c). The slight decrease of ε_{Nd} values in the Hanoi Basin at ∼11 Ma indicates that river drainage adjustment or erosion pattern change still continued in the Red River drainage.

5.3. Tectonic-Landscape-River Drainage in East Asia
The surface uplift of the Tibetan Plateau has significantly influenced the landforms and drainage systems during the Cenozoic in East Asia (Clark et al., 2005; Clift et al., 2006a; Kirby et al., 2002; Richardson et al., 2010; Zheng et al., 2013). Thermochronologic data suggest that a major deformation and exhumation along the eastern margin of plateau occurred by Oligocene-Miocene (Hoke et al., 2014; Tapponnier et al., 2001). The drainage reversal in the central Yangtze basin prior to ∼25 Ma was further linked to the uplift and expansion of the SE margin of Tibet (Clift et al., 2006a; Zheng et al., 2013), indicating an initial topographic

reversal of East Asia (Figure 11b). Meanwhile significant extension led to the formation of a series of small rift basins along the continental margin of South China (Ru & Pigott, 1986) followed by seafloor spreading westward since ~37 Ma (Hsu et al., 2004; Lan et al., 2014). The episode of headward expansion of the Pearl and Minjiang River systems into the continental interior since ~25 Ma can be logically linked with the opening of the South China Sea (Figure 12b). Temporal correlation between a change of topography and drainage systems in southeast China and eastern Tibetan Plateau indicates a regional systematic change in East Asia since ~25 Ma although any geodynamic connection between the uplift of Tibetan Plateau and opening of the South China Sea is still unclear, if it exists at all.

A growing number of thermochronologic studies from deep river gorges in eastern Tibetan Plateau show another rapid cooling and strong river incision since 15–10 Ma (Clark et al., 2005; Kirby et al., 2002). Thermal history modeling of the combined FT and (U-Th)/He data sets show that the southern margin of the South China Block experienced a three stage cooling history. The final-stage cooling event (15–10 Ma) has been documented in the southeast margin of the South China Block synchronously (Yan et al., 2009). Uplift of the eastern Tibetan Plateau and the Wuyi-Nanling Mountains in SE China around 15–10 Ma significantly modified the landscape and river drainage erosion patterns in East Asia (Figure 12c; Yan et al., 2009). The coincidence between rapid cooling of eastern Tibetan Plateau and South China Block at 15–10 Ma indicates that the whole region was affected by the erosional event (Figure 11c). This inferred readjustment of erosion patterns and drainage systems was most likely associated with enhanced Late Miocene uplift of the Tibetan Plateau to the W-NW (Clark et al., 2005; Kirby et al., 2002) and the collisional uplift of the Taiwan Orogen (Huang et al., 1997).

6. Conclusions

The sedimentary records from the northern margin of the South China Sea offer important clues on the major changes in landscape development, river dynamics, and drainage basin evolution in East Asia. Our results demonstrate that the fluvial dynamics of East Asian rivers responded to tectonically induced regional topographic changes swiftly within short periods of geological time. The progressive uplift of the eastern Tibetan Plateau and the opening of the South China Sea ~30–25 Ma were the first-order factors controlling the initiation and development of major river systems in East Asia. Early rivers related to the progressive westward opening of the South China Sea, drain Mesozoic crystalline rocks in the southernmost parts of Cathaysia. Their headward propagation into northern Cathaysia and the interior of the Yangtze block during the Oligocene produced sediments derived from Precambrian-Paleozoic basement units that became even more abundant in the Miocene strata now preserved in the South China Sea. A second pulse of uplift in the eastern Tibetan Plateau and the crustal exhumation of the Wuyi and Nanling Mountains after 15–10 Ma caused significant changes in the regional topography and river drainage erosion patterns in SE China. The modern Pearl River and MinJiang River drainage system was established by ~11 Ma.

References

An, Y. F., Han, Z. J., & Wan, J. L. (2008). Fission track dating of the Cenozoic uplift in Mabian area, southern Sichuan Province. *Science China Earth Sciences*, *51*(9), 1238–1247.

Beyssac, O., Simoes, M., Avouac, J. P., Farley, K. A., Chen, Y.-G., Chan, Y.-C., et al. (2007). Late Cenozoic metamorphic evolution and exhumation of Taiwan. *Tectonics*, *26*, TC6001. https://doi.org/10.1029/2006TC002064

Black, L. P., Kamo, S. L., Allen, C. M., Aleinikoff, J. N., Davis, D. W., Korsch, R. J., et al. (2003). TEMORA 1: A new zircon standard for Phanerozoic U-Pb geochronology. *Chemical Geology*, *200*(1–2), 155–170.

Briais, A., Patriat, P., & Tapponnier, P. (1993). Updated interpretation of magnetic anomalies an seafloor spreading stages in the South China Sea: Implications for the tertiary tectonics of Southeast Asia. *Journal of Geophysical Research*, *98*(B4), 6299–6328.

Brookfield, M. E. (1998). The evolution of the great river systems of southern Asia during the Cenozoic India-Asia collision; rivers draining southwards. *Geomorphology*, *22*(3–4), 285–312.

Carter, A., Roques, D., Bristow, C., & Kinny, P. (2001). Understanding Mesozoic accretion in Southeast Asia: Significance of Triassic thermotectonism (Indosinian orogeny) in Vietnam. *Geology*, *29*(3), 211–214.

Chen, J. F., & Jahn, B. M. (1998). Crustal evolution of southeastern China: Nd and Sr isotopic evidence. *Tectonophysics*, *284*(1–2), 101–133.

Chung, S.-L., Cheng, H., Jahn, B-M., O'Reilly, S. Y., & Zhu, B. (1997). Major and trace element, and Sr-Nd isotope constraints on the origin of Paleogene volcanism in South China prior to the South China Sea opening. *Lithos*, *40*(2–4), 203–220.

Clark, M. K., House, M. A., Royden, L. H., Whipple, K. X., Burchfiel, B. C., Zhang, X., et al. (2005). Late Cenozoic uplift of eastern Tibet. *Geology*, *33*(6), 525–528. https://doi.org/10.1130/G21265.1

Clift, P. D., Blusztajn, J., & Nguyen, D. A. (2006a). Large-scale drainage capture and surface uplift in eastern Tibet before 24 Ma. *Geophysical Research Letters*, *33*, L19403. https://doi.org/10.1029/2006GL027772

Clift, P. D., Carter, A., Campbell, I. H., Pringle, M. S., Lap, N. V., Allen, C. M., et al. (2006b). Thermochronology of mineral grains in the Red and Mekong Rivers, Vietnam: Provenance and exhumation implications for Southeast Asia. *Geochemistry, Geophysics, Geosystems*, *7*, Q10005. https://doi.org/10.1029/2006GC001336

Clift, P. D., Layne, G. D., & Blusztajn, J. (2004). Marine sedimentary evidence for monsoon strengthening, Tibetan uplift and drainage evolution in East Asian. In P. Clift (Ed.), *Continent ocean interactions within East Asian Marginal Seas*, Geophysical Monograph Series (Vol. 149, pp. 255–282). Washington, DC: American Geophysical Union.

Darbyshire, D. P. F., & Sewell, R. J. (1997). Nd and Sr isotope geochemistry of plutonic rocks from Hong Kong: Implications for granite petrogenesis, regional structure and crustal evolution. *Chemical Geology*, *143*(1–2), 81–93.

Fang, Z., Zhao, J. X., & McCulloch, M. T. (1992). Geochemical and Nd isotopic study of Palaeozoic bimodal volcanics in Hainan Island, South China: Implications for rifting tectonics and mantle reservoirs. *Lithos*, *29*(1–2), 127–139.

Gilder, S., Gill, J., Coe, R. S., Zhao, X. X., Liu, Z. W., Wang, G. X., et al. (1996). Isotopic and paleomagnetic constraints on the Mesozoic tectonic evolution of South China. *Journal of Geophysical Research*, *101*(B7), 16137–16154.

Godard, V., Pik, R., Lavé, J., Cattin, R., Tibari, B., Sigoyer, J. D., et al. (2009). Late Cenozoic evolution of the central Longmen Shan, eastern Tibet: Insight from (U-Th)/He thermochronometry. *Tectonics*, *28*, TC5009. https://doi.org/10.1029/2008TC002407

Goldstein, S. L., O'Nions, R. K., & Hamilton, P. J. (1984). A Sm-Nd isotopic study of atmospheric dusts and particulates from major river systems. *Earth and Planetary Science Letters*, *70*(2), 221–236.

Hamilton, P. J., O'Nions, R. K., Bridgwater, D., & Nutman, A. (1983). Sm-Nd studies of Archean metasedimentts and metavolcanics from west Greenland and their implication for the earth's early history. *Earth and Planetary Science Letters*, *62*(2), 263–272.

He, M. Y., Zheng, H. B., Bookhagen, B., & Clift, P. D. (2014). Controls on erosion intensity in the Yangtze River basin tracked by U-Pb detrital zircon dating. *Earth-Science Reviews*, *136*, 121–140.

Hoang, L. V., Wu, F. Y., Clift, P. D., Wysocka, A., & Swierczewska, A. (2009). Evaluating the evolution of the Red River System based on in-situ U-Pb dating and Hf isotope analysis of zircons. *Geochemistry, Geophysics, Geosystems*, *10*, Q11008. https://doi.org/10.1029/2009GC002819

Hoke, G. D., Zeng, J. L., Hren, M. T., Wissink, G. K., & Garzione, C. N. (2014). Stable isotopes reveal high southeast Tibetan Plateau margin since the Paleogene. *Earth and Planetary Science Letters*, *394*, 270–278.

Hsu, S. K., Yeh, Y. C., Doo, W. B., & Tsai, C. H. (2004). New bathymetry and magnetic lineations identifications in the northernmost South China Sea and their tectonic implications. *Marine Geophysical Researches*, *25*(1–2), 29– 44.

Hsu, W. H., Byrne, T. B., Ouimet, W., Lee, Y. H., Chen, Y. G., Soest, M. V., et al. (2016). Pleistocene onset of rapid, punctuated exhumation in the eastern Central Range of the Taiwan orogenic belt. *Geology*, *44*(9), 719–722.

Hu, D., Clift, P. D., Boning, P., Hannigan, R., Hillier, S., Blusztajn, J., et al. (2013). Holocene evolution in weathering and erosion patterns in the Pearl River delta. *Geochemistry, Geophysics, Geosystems*, *14*(7), 2349–2368. https://doi.org/10.1002/ggge.20166

Huang, C.-Y., Wu, W. Y., Chang, C. P., Tsao, S., Yuan, P. B., Lin, C. W., et al. (1997). Tectonic evolution of accretionary prism in the arccontinent collision terrane of Taiwan. *Tectonophysics*, *281*(1–2), 31–51.

Huang, C.-Y., Yen, Y., Zhao, Q., & Lin, C.-T. (2012). Cenozoic stratigraphy of Taiwan: Looking into rifting, stratigraphy and paleoceanography of South China Sea. *Chinese Science Bulletin*, *57*(24), 3130–3149. https://doi.org/10.1007/s11434-012-5349-y

Hurford, A. J. (1990). Standardization of fission track dating calibration: Recommendation by the Fission Track Working Group of the IUGS subcommission on geochronology. *Chemical Geology*, *80*(2), 171–178.

Kirby, E., Reiners, P. W., Krol, M. A., Whipple, K. X., Hodges, K. V., Farley, K. A., et al. (2002). Late Cenozoic evolution of the eastern margin of the Tibetan Plateau: Inferences from 40Ar/39Ar and (U-Th)/He thermochronology. *Tectonics*, *21*(1), 1001. https://doi.org/10.1029/2000TC001246

Lan, C. Y., Chung, S. L., Shen, J. J. S., Lo, C. H., Wang, P. X., Hoa, T. T., et al. (2000). Geochemical and Sr-Nd isotopic characteristics of granitic rocks from northern Vietnam. *Journal of Asian Earth Sciences*, *18*(3), 267–280.

Lan, Q., Yan, Y., Huang, C. Y., Clift, P. D., Li, X. J., Chen, W. H., et al. (2014). Tectonics, topography, and river system transition in East Tibet: Insights from the sedimentary record in Taiwan. *Geochemistry, Geophysics, Geosystems*, *15*, 3658–3674. https://doi.org/10.1002/2014GC005310

Lei, Y. L., Ji, J. Q., Gong, D. H., Zhong, D. L., Wang, X. S., Zhang, J., et al. (2006). Therml and denudational history of granitoid batholith recorded by apatite fission track in the Dulong River region in northwestern Yunnan, since Late Miocene. *Acta Petrologica Sinica*, *22*(4), 938–948.

Lei, Y. L., Zhong, D. L., Jia, C. Z., Ji, J. Q., & Zhang, J. (2008). Late Cenozoic differential uplift-exhumation of batholith and propagation of uplift recorded by fission track thermochronology in Chayu area, the southeast margin of the Tibetan plateau. *Acta Petrologica Sinica*, *24*(2), 384–394.

Li, F. X., & Ma, D. Q. (1991). *Huangling granitic batholith: The emplacement sequence, timing and petrogenesis*. Yichang Institute of Geology and Mineral Resources Report (unpublished report, pp. 90–101), Yichang, Hubei, China.

Li, X. M., Wang, Y. J., Tan, K. X., & Peng, T. P. (2005). Meso-Cenozoic uplifting and exhumation on Yunkaidashan: Evidence from fission track thermochronology. *Chinese Science Bulletin*, *50*(9), 903–909.

Li, X. H. (2000). Cretaceous magmatism and lithospheric extension in southeast China. *Journal of Asian Earth Sciences*, *18*(3), 293–305. https://doi.org/10.1016/S1367-9120(99)00060-7

Li, X. H., Liu, D. Y., Sun, M., Li, W. X., Liang, X. R., & Liu, Y. (2004). Precise Sm-Nd and U-Pb isotopic dating of the super-giant Shizhuyuan polymetallic deposit and its host granite, Southeast China. *Geological Magazine*, *141*(2), 225–231.

Li, X. H., Wei, G. J., Shao, L., Liu, Y., Liang, X. R., Jian, Z. M., et al. (2003). Geochemical and Nd isotopic variations in sediments of the South China Sea: A response to Cenozoic tectonism in SE Asia. *Earth and Planetary Science Letters*, *211*(3–4), 207–220.

Li, Y. Z., Deng, Y. H., Xu, Q., & Yu, X. H. (2010). Sedimentary environmental evolution of the Cenozoic in China offshore basins. *Acta Sedimentologica Sinica*, *28*(6), 1066–1075.

Li, Z. X., & Li, X. H. (2007). Formation of the 1300 km-wide intracontinental orogen and post-orogenic magmatic province in Mesozoic South China: A flat-slab subduction model. *Geology*, *35*(2), 179–182.

Liao, Z. T., Jiang, X. G., Li, R., & Chen, Y. K. (2005). Research on the tectono-thermal evolution of the baise basin, Guangxi province. *Petroleum Geology & Experiment*, *27*(1), 18–24.

Lin, A. T., Watts, A. B., & Hesselbo, S. P. (2003). Cenozoic stratigraphy and subsidence history of the South China Sea margin in the Taiwan region. *Basin Research*, *15*(4), 453–478.

Liu, Z., Colin, C., Huang, W., Le, K. P., Tong, S., Chen, Z., et al. (2007). Climatic and tectonic controls on weathering in south China and Indochina Peninsula: Clay mineralogical and geochemical investigations from the Pearl, Red, and Mekong drainage basins. *Geochemistry Geophysics Geosystems*, *8*, Q05005. https://doi.org/10.1029/2006GC001490

Ludwig, K. R. (2003). *Isoplot/Ex version 3.00: A geochronological toolkit for Microsoft Excel* (Spec. Publ. 4). Berkeley, CA: Berkeley Geochronology Center.

Ma, C. Q., Ehlers, C., Xu, C. H., Li, A. C., & Yang, K. G. (2000). The roots of the Dabieshan ultrahigh-pressure metamorphic terrane: Constraints from geochemistry and Nd–Sr isotope systematics. *Precambrian Research*, *102*(3–4), 279–301.

Ma, D. Q., Li, Z. C., & Xiao, Z. F. (1997). The constitute, geochronology and geologic evolution of the Kongling complex western Hubei. *Acta Sedimentologica Sinica*, *18*(3), 233–241.

Maluski, H., Lepvrier, C., Jolivet, L., Carter, A., Roques, D., Beyssac, O., et al. (2001). Ar-Ar and fission-track ages in the Song Chay massif: Early Triassic and Cenozoic tectonics in northern Vietnam. *Journal of Asian Earth Sciences*, *19*, 233–248.

Meng, X. W., Liu, Y. G., Shi, X. F., & Du, D. W. (2008). Nd and Sr isotopic compositions of sediments from the Yellow and Yangtze Rivers: Implications for partitioning tectonic terranes and crust weathering of the Central and Southeast China. *Frontiers of Earth Science in China*, *2*(4), 418–426. https://doi.org/10.1007/s11707-008-0054-5

Pearce, N. J. G., Perkins, W. T., Westgate, J. A., Gorton, M. P., Jackson, S. E., Neal, C. R., et al. (1997). A compilation of new and published major and trace element data for NIST SRM 610 and NIST SRM 612 glass reference materials, *Geostandards Newsletters*, *21*(1), 115–144. https://doi.org/10.1111/j.1751-908X.1997.tb00538.x

Qin, G. Q. (2000). Comments on "Discussion on the Upper-Lower Tertiary Boundary in Well BY7-1-1 of the Pearl River Mouth Basin" (in Chinese with English abstract). *Journal of Stratigraphy*, *24*, 387–392.

Richardson, N. J., Densmore, A. L., Seward, D., Wipf, M., & Yong, L. (2010). Did incision of the Three Gorges begin in the Eocene?. *Geology*, *38*(6), 551–554. https://doi.org/10.1130/G30527.1

Ru, K., & Pigott, J. D. (1986). Episodic rifting and subsidence in the South China Sea. *AAPG Bulletin*, *70*, 1136–1155.

Shao, L., Li, C. A., Zhang, Y. F., Yuan, S. Y., Wang, J. T., Jaing, H. J., et al. (2014). Sr-Nd isotopic compositions of the Upper Yangtze River sediments: Implications for tracing sediment sources. *Acta Sedimentologica Sinica*, *32*(2), 290–295.

Shao, L., Qiao, P. J., Pang, X., Wei, G. J., Li, Q. Y., Miao, W. L., et al. (2009). Nd isotopic variations and its implications in the recent sediments from the northern South China Sea. *Chinese Science Bulletin*, *54*(2), 311–317. https://doi.org/10.1007/s11434-008-0453-8

Shi, X. B., Kohn, B., Spencer, S., Guo, X. W., Li, Y. M., Yang, X. Q., et al. (2011). Cenozoic denudation history of southern Hainan Island, South China Sea: Constraints from low temperature thermochronology. *Tectonophysics*, *504*(1–4), 100–115.

Shi, X. B., Qiu, X. L., Liu, H. L., Chu, Z. Y., & Xia, B. (2006). Cenozoic cooling history of Lincang granitoid batholith, western Yunnan: Evidence from fission track data. *Chinese Journal of Geophysics*, *49*(1), 129–142.

Sláma, J., Košler, J., Condon, D. J., Crowley, J. L., Gerdes, A., Hanchar, J. M., et al. (2008). Plezovice zircon: A new natural reference material for U-Pb and Hf isotopic microanalysis. *Chemical Geology*, *249*(1–2), 1–35. https://doi.org/10.1016/j.chemgeo.2007.11.005

Tapponnier, P., Xu, Z. Q., Francüoise, R., Bertrand, M., Nicolas, A., Gerard, W., et al. (2001). Oblique stepwise rise and growth of the Tibet Plateau. *Science*, *294*(5547), 1671–1677.

Usuki, T., Lan, C. Y., Wang, K. L., & Chiu, H. Y. (2013). Linking the Indochina block and Gondwana during the Early Paleozoic: Evidence from U-Pb ages and Hf isotopes of detrital zircons. *Tectonophysics*, *586*, 145– 159.

Vermeesch, P., Resentini, A., & Garzanti, E. (2016). An R package for statistical provenance analysis. *Sedimentary Geology*, *336*, 14– 25.

Viola, G., & Anczkiewicz, R. (2008). Exhumation history of the Red River shear zone in northern Vietnam: New insights from zircon and apatite fission-track analysis. *Journal of Asian Earth Sciences*, *33*(1–2), 78–90.

Wan, J. L., Li, Q., & Chen, W. H. (1997). Fission track evidence of diachronic uplift along the Ailao Shan-Red River left-lateral strike-slip shear zone. *Seismology and Geology*, *19*(1), 87–90.

Wang, C., Liang, X., Xie, Y., Tong, C., Pei, J., Zhou, Y., et al. (2015). Late Miocene provenance change on the eastern margin of the Yinggehai-Song Hong Basin, South China Sea: Evidence from U-Pb dating and Hf isotope analyses of detrital zircons. *Marine and Petroleum Geology*, *61*, 123–139.

Wang, E., Kirby, E., Furlong, K. P., Soest, M. V., Xu, G., Shi, X., et al. (2012). Two-phase growth of high topography in eastern Tibet during the Cenozoic. *Nature Geoscience*, *5*(9), 640–645.

Wang, Y. H., Wang, S. C., & Kang, T. S. (1994). Zircon and apatite fission track study of the thrust belt in southwest Fujiang provenance. *Chinese Science Bulletin*, *39*(8), 723–726.

Wu, Q. H., Liu, S. S., Jonckheere, R., & Wagner, G. A. (2002). Primary analysis on tectonic implication of apatite fission track ages from eastern Dabie area, china. *Chinese Journal of Geology*, *37*(3), 343–349.

Wu, W., Xu, S. J., Yang, J. D., Yin, H. W., Lu, H. Y., & Zhang, K., J. (2010). Isotopic characteristics of river sediments on the Tibetan Plateau. *Chemical Geology*, *269*(3–4), 406–413. https://doi.org/10.1016/j.chemgeo.2009.10.015

Xu, X. S., O'reilly, S. Y., Griffin, W. L., Wang, X. L., Pearson, N. J., & He, Z. Y. (2007). The crust of Cathaysia: Age, assembly and reworking of two terranes. *Precambrian Research*, *158*(1–2), 51–78.

Xu, Y. H., & Chen, J. (2010). Uranium-lead dating of detrial zircons from the Minjiang and Jiulong Estuaries in the western coast of the Taiwan Strait: Implication for its provenance. *Acta Oceanologica Sinica*, *32*(4), 110–117.

Yan, Y., Carter, A., Xia, B., Lin, G., Brichau, S., & Hu, X. Q. (2009). A fission-track and (U-Th)/He thermochronometric study of the northern margin of the South China Sea: An example of a complex passive margin. *Tectonophysics*, *474*(3–4), 584–594.

Yan, Y., Carter, A., Palk, C., Brichau, S., & Hu, X. (2011). Understanding sedimentation in the Song Hong-Yinggehai Basin, South China Sea. *Geochemistry, Geophysics, Geosystems*, *12*, Q06014. https://doi.org/10.1029/2011GC003533

Yan, Y., Hu, X-Q., Lin, G., Santosh, M., & Chan, L.-S. (2011). Detrital zircon U-Pb data in the Hengyang Basin, South China Block: Implication to Mesozoic landscape and tectonic transition of East Asia. *JAES*, *41*(6), 494–503.

Yan, Y., Xia, B., Lin, G., Carter, A., Hu, X., Cui, X., et al. (2007). Geochemical and Nd isotope composition of detrital sediments on the north margin of the South China Sea: Provenance and tectonic implications. *Sedimentology*, *54*(1), 1–17.

Yang, S., Jiang, S., Ling, H., Xia, X., Sun, M., & Wang, D. (2007). Sr-Nd isotopic compositions of the Changjiang sediments: Implications for tracing sediment sources. *Science in China Series D*, *50*(10), 1556–1565.

Yang, S. Y., Li, C. X., & Yokoyama, K. (2006). Elemental compositions and monazite age patterns of core sediments in the Changjiang Delta: Implications for sediment provenance and development history of the Changjiang River. *Earth and Planetary Science Letters*, *245*(3–4), 762–776.

Zhang, K. J., Zhang, Y. X., Li, B., & Zhong, L. F. (2007). Nd isotopes of siliciclastic rocks from Tibet, western China: Constraints on provenance and pre-Cenozoic tectonic evolution. *Earth and Planetary Science Letters*, *256*(3–4), 604–616. https://doi.org/10.1016/j.epsl.2007.02.014

Zhang, X. C., Huang, C. Y., Wang, Y. J., Clift, P. D., Yan, Y., Fu, X. W., et al. (2017). Evolving Yangtze River reconstructed by detrital zircon U-Pb dating and petrographic analysis of Miocene Marginal Sea sedimentary rocks of the Western Foothills and Hengchun Peninsula, Taiwan. *Tectonics*, *36*, 634–651. https://doi.org/10.1002/2016TC004357

Zhao, M., Shao, L., Liang, J. S., & Li, Q. Y. (2015b). No Red River capture since the late Oligocene: Geochemical evidence from the Northwestern South China Sea. *Deep Sea Research, Part II*, *122*, 185–194.

Zhao, M., Shao, L., & Qiao, P. J. (2015a). Characteristics of detrital Zircon U-Pb geochronology of the Pearl River Sands and its implication on provenances. *Journal of Tongji University (Natural Science)*, *43*(6), 915–923. https://doi.org/10.11908/j.issn.0253-374x.2015.06.018

Zheng, H. B., Clift, P. D., Wang, P., Tada, R., Jia, J. T., He, M. Y., et al. (2013). Pre-Miocene birth of the Yangtze River. *Proceedings of the National Academy of Sciences of the United Stated of America*, https://doi.org/10.1073/pnas.1216241110***

Zhong, L. F., Li, G., Yan, W., Xia, B., Feng, Y. X., Miao, L., et al. (2017). Using zircon U-Pb ages to constrain the provenance and transport of heavy minerals within the northwestern shelf of the South China Sea. *Journal of Asian Earth Sciences*, *134*, 176–190.

Zhou, H., Xiao, L., Dong, Y., Wang, C., Wang, F., & Ni, P. (2009). Geochemical and geochronological study of the Sanshui basin bimodal volcanic rock suite, China: Implications for basin dynamics in southeastern China. *Journal of Asian Earth Science*, *34*(2), 178–189.

Zhou, Z. Y., Guo, T. L., Xu, C. H., & Yang, F. L. (2005). Fission Track Analysis on Mesozoic Strata in the Shiwandashan Basin, Guangxi Province and Its Geological Significance. *Acta Geologica Sinica*, *79*(3), 395–401.

Zhou, Z. Y., Xu, C. H., Reiners, P. W., Yang, F. L., & Donelick, R. A. (2003). Late Cretaceous erosion history in Tiantangzhai area of Dabie Orogen: (U-Th)/He and fission track study. *Chinese Science Bulletin*, *48*(11), 1151–1602.